

## Retroviral Nucleocapsid Proteins Display Nonequivalent Levels of Nucleic Acid Chaperone Activity<sup>∇</sup>

Kristen M. Stewart-Maynard,<sup>1</sup> Margareta Cruceanu,<sup>2</sup> Fei Wang,<sup>2</sup> My-Nuong Vo,<sup>1</sup> Robert J. Gorelick,<sup>3</sup> Mark C. Williams,<sup>2</sup> Ioulia Rouzina,<sup>4\*</sup> and Karin Musier-Forsyth<sup>5\*</sup>

*Department of Chemistry and Institute for Molecular Virology, University of Minnesota, Minneapolis, Minnesota 55455<sup>1</sup>; Department of Physics, Northeastern University, Boston, Massachusetts 02115<sup>2</sup>; AIDS Vaccine Program, Basic Research Program, SAIC-Frederick, Incorporated, National Cancer Institute-Frederick, Frederick, Maryland 21702<sup>3</sup>; Department of Molecular Biology, Biochemistry and Biophysics, University of Minnesota, Minneapolis, Minnesota 55455<sup>4</sup>; and Departments of Chemistry and Biochemistry, The Ohio State University, Columbus, Ohio 43210<sup>5</sup>*

Received 4 June 2008/Accepted 29 July 2008

**Human immunodeficiency virus type 1 (HIV-1) nucleocapsid protein (NC) is a nucleic acid chaperone that facilitates the remodeling of nucleic acids during various steps of the viral life cycle. Two main features of NC's chaperone activity are its abilities to aggregate and to destabilize nucleic acids. These functions are associated with NC's highly basic character and with its zinc finger domains, respectively. While the chaperone activity of HIV-1 NC has been extensively studied, less is known about the chaperone activities of other retroviral NCs. In this work, complementary experimental approaches were used to characterize and compare the chaperone activities of NC proteins from four different retroviruses: HIV-1, Moloney murine leukemia virus (MLV), Rous sarcoma virus (RSV), and human T-cell lymphotropic virus type 1 (HTLV-1). The different NCs exhibited significant differences in their overall chaperone activities, as demonstrated by gel shift annealing assays, decreasing in the order HIV-1 ~ RSV > MLV >> HTLV-1. In addition, whereas HIV-1, RSV, and MLV NCs are effective aggregating agents, HTLV-1 NC, which exhibits poor overall chaperone activity, is unable to aggregate nucleic acids. Measurements of equilibrium binding to single- and double-stranded oligonucleotides suggested that all four NC proteins have moderate duplex destabilization capabilities. Single-molecule DNA-stretching studies revealed striking differences in the kinetics of nucleic acid dissociation between the NC proteins, showing excellent correlation between nucleic acid dissociation kinetics and overall chaperone activity.**

Retroviral nucleocapsid proteins (NCs) are small polypeptides containing a large number of basic residues and one or two invariant CCHC metal-ion binding motifs (11, 44, 52). In particular, human immunodeficiency virus type 1 (HIV-1) NC is a 55-amino-acid protein containing a basic N-terminal domain and two zinc fingers separated by a short basic linker (Fig. 1a) (27, 67, 89). HIV-1 NC is a multifunctional nucleic acid binding protein that has been shown to play a role in numerous steps in the viral life cycle, including RNA genome dimerization (26, 39, 42, 85), genomic-RNA packaging (13), reverse transcription (22, 27, 89, 99), tRNA primer annealing (20, 21, 29, 38, 47, 48, 86), and DNA integration (19, 43).

Many steps in the HIV-1 life cycle rely on NC's ability to function as a nonspecific nucleic acid chaperone that facilitates the rearrangement of nucleic acids into thermodynamically more stable conformational states (22, 53, 67, 89, 99). The chaperone function of HIV-1 NC is derived from two independent activities, nucleic acid aggregation (66, 98) and weak-

duplex destabilization (7–10, 14, 23, 46, 47, 58, 79, 100, 101, 107, 110), which are associated with the N-terminal cationic domain and the zinc fingers, respectively. Recently, rapid kinetics of nucleic acid dissociation was shown to be another key feature of NC's chaperone function (23).

Whereas HIV-1 NC's nucleic acid chaperone activity has been extensively studied, relatively little is known about the chaperone activities of other retroviral NCs. In this work, complementary experimental approaches were used to compare the chaperone activity of HIV-1 NC (also known as NCp7) to those of Rous sarcoma virus (RSV) NCp12, Moloney murine leukemia virus (MLV) NCp10, and human T-cell lymphotropic virus type 1 (HTLV-1) NCp15 (Fig. 1a). By studying the chaperone activities of various NCs, a better understanding of all retroviral NCs, as well as the differences between the retroviruses, will be obtained. The NCs shown in Fig. 1a were chosen for a number of reasons. First, there are distinct structural differences between them, including differences in the number of zinc fingers, the number and location of aromatic and basic residues, and the overall charge of the proteins. Second, the R terminal-repeat regions among the genomes of these retroviruses differ significantly in length and structural complexity. The complementary R regions present in minus-strand DNA and viral RNA are annealed following minus-strand strong-stop DNA synthesis. HIV-1 NC has been shown to greatly stimulate this process by annealing and blocking a competing

\* Corresponding author. Mailing address for Karin Musier-Forsyth: Department of Chemistry, The Ohio State University, 100 W 18th Ave., Columbus, OH 43210. Phone: (614) 292-2021. Fax: (614) 688-5402. E-mail: musier@chemistry.ohio-state.edu. Mailing address for Ioulia Rouzina: Department of Molecular Biology, Biochemistry, and Biophysics, University of Minnesota, Minneapolis, MN 55455. Phone: (612) 624-7468. Fax: (612) 625-2163. E-mail: rouzi002@umn.edu.

<sup>∇</sup> Published ahead of print on 6 August 2008.

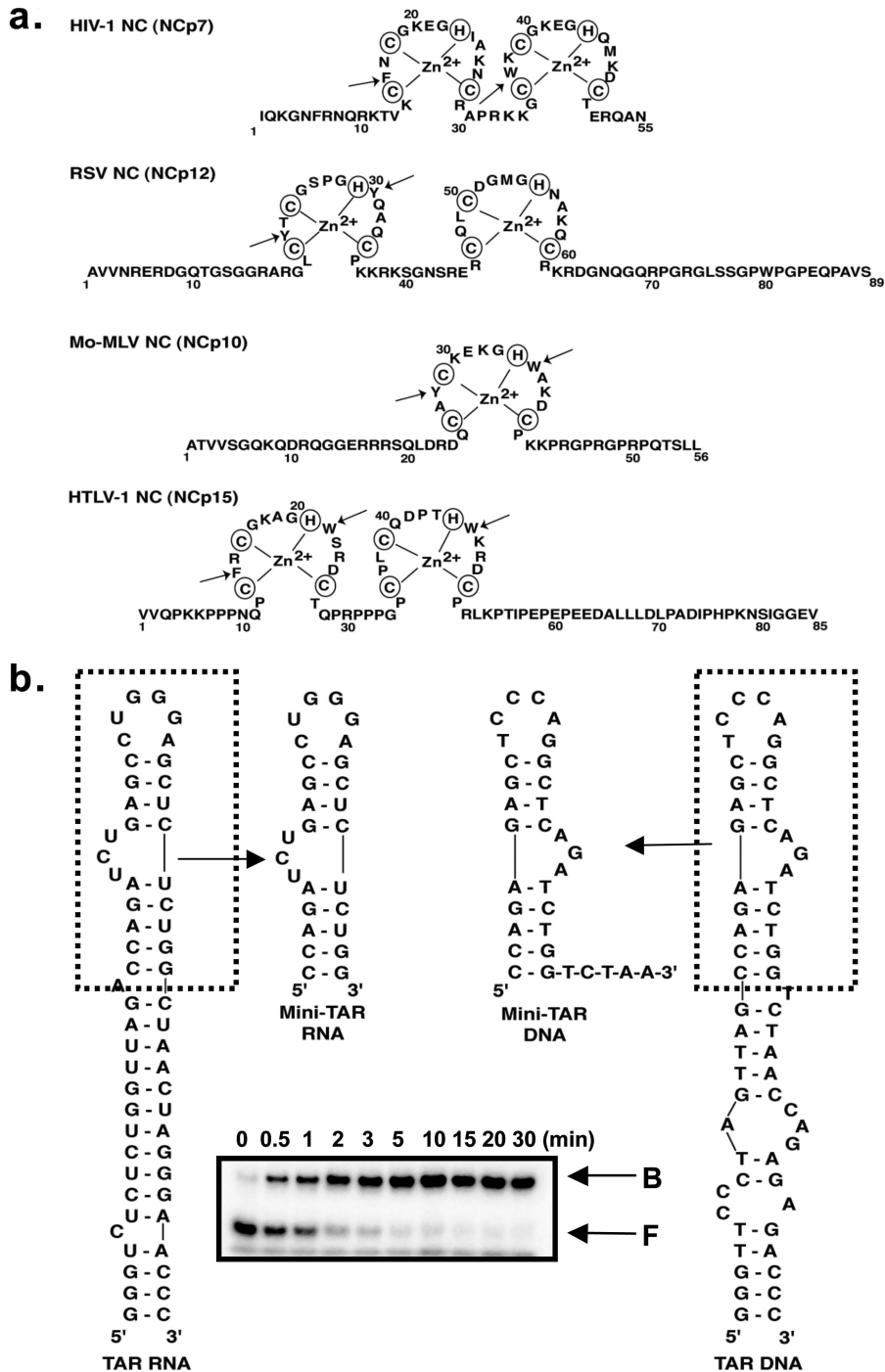


FIG. 1. (a) Sequences of HIV-1, RSV, MLV, and HTLV-1 NCs. Zinc-binding residues are circled. The arrows point to aromatic residues. (b) Predicted secondary structures of full-length TAR and mini-TAR RNA and DNA hairpins. The sequences are derived from the HIV-1 NL4-3 isolate. The mini-TAR constructs are derived from the top part of the hairpin (dotted boxes). Mini-TAR DNA contains an additional 5-nt single-stranded overhang. The secondary structures were predicted by *m*-fold analysis (114). (Inset) Typical mini-TAR gel shift analysis performed as a function of time. The arrow labeled F indicates the position of free mini-TAR RNA, and the arrow labeled B points to the mini-TAR RNA/DNA binary complex.

self-priming reaction (18, 33, 45, 51, 54, 65, 68). Based on the structural differences in the R regions, the roles of the other retroviral NC proteins in minus-strand transfer and prevention of self-priming may differ significantly. Finally, the NC proteins studied in this work come from retroviruses belonging to four

different genera, each of which is only distantly related to the other three.

Here, we examined the annealing kinetics of complementary hairpin molecules derived from the top of the 59-nucleotide (nt) *trans*-activation response element (TAR) hairpin se-

quence that is part of the R region of the HIV-1 genome (Fig. 1b) using gel shift assays. The aggregation abilities of the different NCs were tested using a simple sedimentation assay. Fluorescence anisotropy (FA) measurements were performed to determine the relative binding affinities of these NC proteins to nucleic acids. Finally, single-molecule DNA-stretching studies were carried out to probe the effect of each protein on force-induced DNA melting, which provides information on the effects of different NCs on DNA duplex stability and on the kinetics of protein-DNA interactions.

## MATERIALS AND METHODS

**Protein and nucleic acid preparation.** HIV-1 NC was prepared either by solid-phase synthesis (69) or by recombinant methods, as described previously (19, 46). The gene for RSV NC was PCR amplified from the RCASBP(B) vector, a generous gift from Stephen H. Hughes (National Cancer Institute-Frederick, Frederick, MD) (55) and cloned into pET32a (Novagen, Madison, WI) using standard molecular biology methods. The resulting clone, pDB1023, expressed RSV NCp12 as a thioredoxin fusion and used an enterokinase (DDDK) cleavage site to liberate authentic RSV NCp12. The expression plasmid for MLV NCp10, pDB1056, was prepared by insertion of the MLV NC sequence (GenBank accession no. J02255) into pET32a with an enterokinase site encoded between thioredoxin and NC. The gene encoding HTLV-1 NCp15 was PCR amplified from a full-length HTLV-1 proviral plasmid, pCS-HTLV-1 (30) (a generous gift from David Derse, National Cancer Institute-Frederick), and cloned into pET32a to generate the plasmid pDR2559, which expresses HTLV-1 NCp15 as a thioredoxin fusion with a tobacco etch virus protease cleavage site (ENLYFQ) (59, 60) to liberate authentic HTLV-1 NC. RSV, MLV, and HTLV-1 NCs were expressed, isolated, and purified essentially as described previously (19, 46). The NCs were stored in lyophilized forms at  $-80^{\circ}\text{C}$ . Prior to use, the proteins were resuspended in diethylpyrocarbonate (DEPC)-treated water or NC storage buffer [20 mM HEPES, 5 mM  $\beta$ -mercaptoethanol, 0.1 mM Tris(2-carboxyethyl)-phosphine hydrochloride, pH 7.5]. NC concentrations were determined by measuring the absorbance at 280 nm ( $A_{280}$ ) and using the following extinction coefficients: HIV-1 NC,  $6,050 \text{ M}^{-1} \text{ cm}^{-1}$ ; RSV NC,  $8,430 \text{ M}^{-1} \text{ cm}^{-1}$ ; MLV NC,  $6,970 \text{ M}^{-1} \text{ cm}^{-1}$ ; HTLV-1 NC,  $11,740 \text{ M}^{-1} \text{ cm}^{-1}$ .

The mini-TAR RNA construct was obtained from Dharmacon (Lafayette, CO), and the mini-TAR DNA construct was obtained from Integrated DNA Technologies (Coralville, IA). The mini-TAR RNA and DNA oligonucleotides were purified on 16% denaturing polyacrylamide gels, dissolved in DEPC-treated water, and stored at  $-20^{\circ}\text{C}$ . Oligonucleotide concentrations were determined by the  $A_{260}$  using the following extinction coefficients: mini-TAR RNA,  $2.82 \times 10^5 \text{ M}^{-1} \text{ cm}^{-1}$ ; mini-TAR DNA,  $3.06 \times 10^5 \text{ M}^{-1} \text{ cm}^{-1}$ .

Mini-TAR RNA was radiolabeled with [ $\gamma$ - $^{32}\text{P}$ ]ATP (Perkin-Elmer Life and Analytical Sciences, Waltham, MA) and T4 polynucleotide kinase (New England Biolabs, Ipswich, MA) using standard protocols. The radiolabeled TAR constructs were purified on 16% denaturing polyacrylamide gels, dissolved in DEPC-treated water, and stored at  $-20^{\circ}\text{C}$ .

Prior to use, the mini-TAR oligonucleotides were refolded in 25 mM HEPES, pH 7.5, and 100 mM NaCl at a concentration that was 100-fold greater than the final assay concentration. The oligonucleotides were incubated at  $80^{\circ}\text{C}$  for 2 min and cooled to  $60^{\circ}\text{C}$  for 2 min, followed by the addition of  $\text{MgCl}_2$  to 10 mM and placement on ice for at least 5 min.

**Annealing assays.** Steady-state annealing assays were performed to determine the amount of NC required to reach saturating annealing levels. Solutions containing 15 nM refolded  $^{32}\text{P}$ -labeled mini-TAR RNA and 45 nM refolded mini-TAR DNA in reaction buffer (20 mM HEPES, pH 7.5, 20 mM NaCl, 5 mM dithiothreitol, and 0.2  $\text{MgCl}_2$ ) were incubated for 5 min at  $37^{\circ}\text{C}$ . NC was then added to final concentrations varying from 0.5 to 5  $\mu\text{M}$ , and the reaction mixtures were incubated for 30 min at  $37^{\circ}\text{C}$ . The reactions were quenched by incubation with 1% (vol/vol) sodium dodecyl sulfate (SDS) for 5 min at room temperature, followed by placement on ice. Samples were extracted twice with 4:1 phenol-chloroform and then analyzed on 15% SDS-polyacrylamide gels (375 mM Tris-HCl, pH 8.8, 0.1% SDS, 19:1 [wt/vol] acrylamide-bisacrylamide) run at  $25^{\circ}\text{C}$  in Tris-glycine (25 mM Tris, 250 mM glycine, pH 8.3) running buffer. Following overnight exposure to phosphor screens, the gels were visualized using a Bio-Rad Molecular Imager FX and analyzed using Bio-Rad Quantity One software.

Annealing assays to determine the kinetics of mini-TAR RNA and DNA annealing were performed in the presence of 1.5  $\mu\text{M}$  HIV-1 NC (1.2 nt-to-NC ratio), 1.0  $\mu\text{M}$  RSV NC (1.8 nt/NC), 3.0  $\mu\text{M}$  MLV NC (0.6 nt/NC), or 3.0  $\mu\text{M}$

HTLV-1 NC (0.6 nt/NC). For assays carried out over a 30-min period, 5 nM or 15 nM mini-TAR RNA and various concentrations of mini-TAR DNA (indicated in the figure legends) were incubated for 5 min at  $37^{\circ}\text{C}$  in reaction buffer prior to the addition of NC. Following the addition of NC, aliquots from the reaction mixture were removed and quenched by the addition of SDS to a final concentration of 1% (vol/vol), incubated at room temperature for 5 min, and then placed on ice. Samples were analyzed as described above. For assays carried out over a 120-min period, separate reaction mixtures containing mini-TAR RNA and mini-TAR DNA in reaction buffer were prepared and preincubated at  $37^{\circ}\text{C}$  (unless otherwise noted in the figure legends) prior to the addition of NC. The reactions were quenched at the specified time points and analyzed as described previously.

**Sedimentation/aggregation assays.** Solutions containing refolded  $^{32}\text{P}$ -labeled mini-TAR RNA (15 nM) and mini-TAR DNA (45 nM) were prepared in reaction buffer. NC was added to concentrations of 0.25, 0.5, 1.25, 2.5, and 5.0  $\mu\text{M}$  (7.2, 3.6, 1.4, 0.7, and 0.4 nt/NC, respectively), and samples were incubated at  $37^{\circ}\text{C}$  for 30 min. The samples were then centrifuged at  $13,400 \times g$  (12,000 rpm; IEC Micromax RF) at  $4^{\circ}\text{C}$  for 20 min, and an aliquot of the supernatant (5  $\mu\text{l}$ ) was analyzed by scintillation counting. The percent radioactivity remaining in solution relative to a sample measured in the absence of NC (set to 100%) was plotted as a function of the NC concentration.

**FA experiments.** Equilibrium binding of HIV-1, RSV, MLV, and HTLV-1 NCs to a 6-carboxyfluorescein (FAM)-labeled 20-nt single-stranded DNA (ssDNA) oligonucleotide (5'-FAM-CTTCTTTGGGAGTGAATTAG-3') was examined using FA. The high-performance liquid chromatography-purified DNA oligomer (5'-FAM DNA20) was from TriLink Biotechnologies (San Diego, CA). Binding to the corresponding 20-nt RNA/DNA hybrid duplex was also measured. The high-performance liquid chromatography-purified RNA oligomer (5'-CUAAUUCACUCCCAAGAAG-3') was from Dharmacon. FA measurements were performed on an Analyst AD plate reader system (Molecular Devices, Sunnyvale, CA) using Corning 3676 low-volume 384-well black nonbinding-surface polystyrene plates. The reaction mixtures contained 20 nM 5'-FAM DNA20 or the RNA/DNA duplex, various concentrations of NC (0 to 10.2  $\mu\text{M}$ , i.e., to 0.04 or 0.08 nt/NC for DNA or DNA/RNA experiments, respectively), and a final buffer consisting of 20 mM HEPES, pH 7.5, 50 mM NaCl, 5 mM  $\beta$ -mercaptoethanol, 1  $\mu\text{M}$   $\text{ZnCl}_2$ , 100  $\mu\text{M}$  Tris(2-carboxyethyl)phosphine, and 1 mM dithiothreitol. Samples were excited at 485 nm, and the emission intensities at 530 nm from the parallel and perpendicular planes were measured. Equilibrium dissociation constants ( $K_d$ ) were determined by fitting the FA signal,  $A$ , as a function of the protein concentration,  $C$ , with respect to  $K_d$  using the following expression (25, 64, 70):

$$A(C) = \frac{A_F + \Theta \cdot (A_{BR} - A_F)}{\Theta \cdot (R - 1) + 1} \quad (1)$$

where

$$\Theta = \frac{1}{2D} \cdot [D + C + K_d - \sqrt{(D + C + K_d)^2 - 4C \cdot D}]$$

is the fraction of oligonucleotides bound,  $D$  is the oligonucleotide strand concentration, and  $A_B$  and  $A_F$  are the anisotropy values of the fully bound and unbound oligonucleotides, respectively.  $R$  is the ratio of the fluorescence intensity of saturated bound oligonucleotide relative to free oligonucleotide, which accounts for changes in fluorescence intensity upon NC binding (25, 40, 70). Equation 1 assumes 1:1 oligomer-protein binding.

**Single-molecule DNA stretching.** The optical-tweezers instrument, preparation of biotinylated  $\lambda$ -DNA, and data acquisition were described previously (107, 110). The DNA was labeled at the 3' ends so that it would be free to rotate when stretched. The buffer used for the force-induced melting experiments contained 50 mM  $\text{Na}^+$  (10 mM HEPES, 45 mM NaCl, and 5 mM NaOH, pH 7.5). The protein equilibrium dissociation constant,  $K_d$ , was estimated as described previously (25) using the following equation:

$$\frac{1}{K_d} = \frac{1}{\delta F_{\text{sat}}} \cdot \frac{\delta F(c)}{c} = \frac{1}{\delta F_{\text{sat}}} \cdot \left. \frac{d(\delta F(c))}{dc} \right|_{c \rightarrow 0} \quad (2)$$

where  $\delta F(c)$  is the change in the DNA force-induced melting transition width due to the addition of NC at the concentration  $c$ ,  $\Delta F^{\text{sat}}$  is  $\Delta F$  at saturating protein binding, and  $d(\delta F(c))/dc$  is the slope of  $\delta F(c)$  versus  $c$  in the low-concentration (linear) region. The DNA force-induced melting transition width,  $\Delta F$ , is the force range where the force extension curve has the smallest slope corresponding to DNA elongation from its double-stranded to single-stranded form (25).

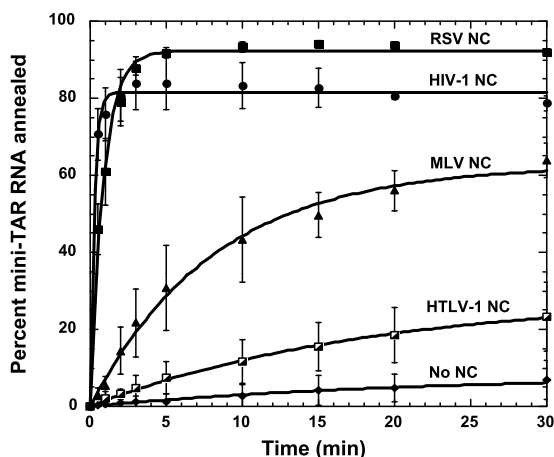


FIG. 2. Annealing time courses for mini-TAR RNA/DNA hairpins. Annealing was performed in the presence of 15 nM RNA and 90 nM DNA at 37°C. The concentrations of NCs used were 1.5  $\mu$ M HIV-1, 1  $\mu$ M RSV, 3  $\mu$ M MLV, and 3  $\mu$ M HTLV-1 (2.1, 3.2, 1, and 1 nt/NC, respectively). The curves represent single-exponential fits to equation 4 with variable final percent annealed product. The error bars indicate standard deviations.

## RESULTS

**Effects of different retroviral NC proteins on mini-TAR RNA/DNA annealing. (i) Mini-TAR RNA/DNA annealing kinetics.** The annealing of mini-TAR RNA and DNA hairpins in the presence of HIV-1, MLV, RSV, and HTLV-1 NCs (Fig. 1a) was studied by gel shift annealing assays using  $^{32}$ P-labeled RNA (Fig. 1b, inset). The predicted secondary structures of HIV-1 TAR RNA (NL4-3 isolate) and TAR DNA hairpins are shown in Fig. 1b. The mini-TAR constructs comprise the top portions of the TAR hairpins and contain the main structural features of TAR. Quantification of the band intensities provides the percentage of RNA molecules annealed as a function of time,  $P(t)$ . In the absence of a protein chaperone, annealing of mini-TAR RNA and DNA involves the fast formation of an extended kissing-loop intermediate, followed by slow conversion to the product duplex (104). The apparent kinetics of mini-TAR RNA/DNA annealing can be described by the following equation (104):

$$P(t) = P_{\infty} \cdot (f \cdot (1 - e^{-k_f t}) + (1 - f) \cdot (1 - e^{-k_s t})) \quad (3)$$

Here,  $k_f$  and  $k_s$  are the high and low annealing rates, corresponding to formation of the intermediate and the fully annealed duplex, respectively, and  $f$  is the probability of intermediate formation.  $P_{\infty}$  is the equilibrium final percentage of RNA annealed. Under some experimental conditions (e.g., in the presence of saturating levels of HIV, RSV, or MLV NC), the hairpin annealing kinetics becomes effectively single exponential due to fast formation of the stable intermediate. In these cases, the data are fitted to a single-exponential equation:

$$P(t) = P_{\infty} \cdot (1 - e^{-kt}) \quad (4)$$

where  $k$  is the annealing rate.

Figure 2 compares the annealing of mini-TAR RNA/DNA hairpins in the presence of saturating concentrations of HIV-1, RSV, MLV, and HTLV-1 NCs. The amount of NC required to

achieve saturated annealing is indicated in the legend to Fig. 2 and was determined by steady-state annealing assays, as described in Materials and Methods (data not shown). These data suggest that the chaperone activity decreases in the order HIV-1 NC  $\sim$  RSV NC  $>$  MLV NC  $>$  HTLV-1 NC. The effective annealing rates and final percentages of RNA annealed differ considerably for the four NCs studied. Annealing in the presence of RSV NC results in higher plateau levels of duplex product than for HIV-1 NC, and an annealing rate,  $k$ , of  $\sim 1.0 \text{ min}^{-1}$ , which is lower than the  $k$  observed for HIV-1,  $\sim 1.6 \text{ min}^{-1}$  (Table 1). For MLV NC, the annealing rate, 0.15  $\text{min}^{-1}$ , and final annealing levels were markedly reduced relative to those observed for HIV-1 NC and RSV NC. Addition of HTLV-1 NC to the annealing reaction resulted in only minor stimulation of annealing relative to the reaction performed in the absence of protein, with an annealing rate of 0.008  $\text{min}^{-1}$ . Since HTLV-1 NC is a very inefficient nucleic acid chaperone, the annealing kinetics was not investigated further using this method.

To gain further insights into the effects of HIV-1, RSV, and MLV NCs on mini-TAR RNA/DNA annealing, assays were performed in the presence of various DNA concentrations ( $D$ ) (Fig. 3a to c). Rates of mini-TAR RNA/DNA annealing were plotted as a function of  $D$  (Fig. 4), and the effective bimolecular rate constant,  $k_{\text{eff}}$ , was obtained from the initial slopes of these plots.

For mini-TAR RNA/DNA annealing in the absence of NC (104), the dominant low rate of annealing was proportional to  $D$ , and the effective bimolecular association rate constant was  $\sim 100 \text{ M}^{-1} \cdot \text{s}^{-1}$  (Table 1). Addition of saturating amounts of HIV-1 NC resulted in  $\sim 1,000$ -fold overall rate enhancement (Table 1), leading to a  $k_{\text{eff}}$  of  $\sim 3 \times 10^5 \text{ M}^{-1} \cdot \text{s}^{-1}$ . At low  $D$  ( $< 60 \text{ nM}$ ), the annealing rate with RSV NC was higher than with HIV-1 NC (Fig. 4). However, at higher  $D$ , the opposite was true, resulting in a  $k_{\text{eff}}$  of  $\sim 6 \times 10^4 \text{ M}^{-1} \cdot \text{s}^{-1}$  for RSV NC (Table 1).

For MLV NC, the annealing at all  $D$  values was slow compared to annealing with either HIV-1 or RSV NC (Fig. 3c). Both the apparent reaction rate,  $k$ , and the  $k_{\text{eff}}$  were significantly smaller (Table 1 and Fig. 4), suggesting that MLV NC is a relatively poor nucleic acid chaperone compared to HIV-1 or RSV NC.

TABLE 1. Kinetic parameters for annealing of mini-TAR RNA/DNA in the absence and presence of different retroviral NCs

NC	$k$ ( $\text{min}^{-1}$ ) <sup>a</sup>	$k_{\text{eff}}$ ( $\text{M}^{-1} \text{ s}^{-1}$ ) <sup>b</sup>	$\Delta H^\ddagger$ (kcal/mol) <sup>c</sup>
None	0.001	$(1 \pm 0.5) \times 10^2$	$19 \pm 3$
HIV-1	$1.6 \pm 0.3$	$(3 \pm 2) \times 10^5$	$8.3 \pm 2$
RSV	$1.0 \pm 0.2$	$(6 \pm 2) \times 10^4$	$12.8 \pm 2$
MLV	$0.15 \pm 0.05$	$(3 \pm 2) \times 10^4$	$10.5 \pm 3$
HTLV-1	0.008	ND	ND

<sup>a</sup>  $k$  is the annealing rate measured at 37°C in the presence of 15 nM mini-TAR RNA annealing to 90 nM mini-TAR DNA (Fig. 2). The NC concentrations used to achieve saturated binding were as follows: 1.5  $\mu$ M HIV-1 NC (1.2 nt/NC), 1  $\mu$ M RSV NC (1.8 nt/NC), 3  $\mu$ M MLV NC (0.6 nt/NC), and 3  $\mu$ M HTLV-1 NC (0.6 nt/NC). The data for no NC are taken from reference 104.

<sup>b</sup>  $k_{\text{eff}}$  is the effective bimolecular rate constant calculated from the slope of  $k$  versus  $D$  at low  $D$  (Fig. 4).

<sup>c</sup>  $\Delta H^\ddagger$  is the enthalpy of the rate-limiting step of mini-TAR hairpin annealing determined by an Arrhenius analysis according to equation 5.

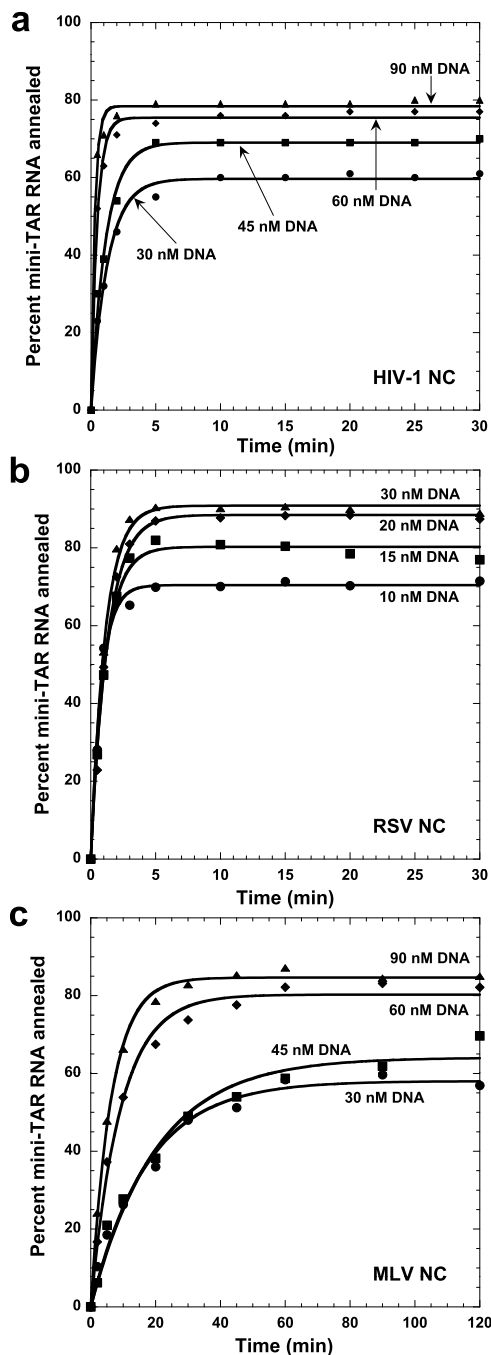


FIG. 3. Annealing time courses of 15 nM mini-TAR RNA to 30 to 90 nM mini-TAR DNA at 37°C in the presence of 1.5  $\mu$ M HIV-1 NC (0.9 to 1.8 nt/NC) (a), 1  $\mu$ M RSV NC (1.35 to 2.7 nt/NC) (b), and 3  $\mu$ M MLV NC (0.45 to 0.9 nt/NC) (c). The curves represent the single-exponential fits to equation 2 with variable final percent annealed product.

(ii) **Temperature dependence of mini-TAR RNA/DNA annealing.** Mini-TAR hairpin annealing rates were enhanced with increasing temperature in both the absence and presence of HIV-1 NC, suggesting that melting of some portion of the mini-TAR hairpin secondary structure is in preequilibrium to bimolecular association (104). A similar enhancement of an-

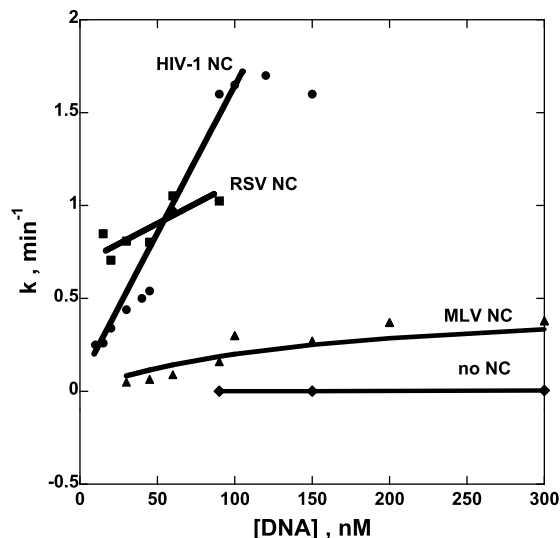


FIG. 4. Rates of mini-TAR RNA/DNA annealing as a function of the mini-TAR DNA concentration in the absence and presence of 1.5  $\mu$ M HIV-1 NC (0.9 to 1.8 nt/NC), 1  $\mu$ M RSV NC (1.35 to 2.7 nt/NC), and 3  $\mu$ M MLV NC (0.45 to 0.9 nt/NC). The lines are guides for the eye, emphasizing linear  $k$ -versus- $D$  relationship at lower  $D$  values. The rates were derived from annealing time courses similar to the ones presented in Fig. 3.

nealing rates with increased temperature was observed in the presence of RSV and MLV NCs. The effect of increased temperature on mini-TAR RNA/DNA annealing in the presence of MLV NC is shown in Fig. 5a. The enthalpy values for the rate-limiting step of annealing,  $\Delta H^\ddagger$ , were obtained according to the Arrhenius expression:

$$\Delta H^\ddagger = -RT \cdot \frac{d \ln(k)}{d(1/T)} \quad (5)$$

where  $R$  is the molar gas constant and  $T$  is temperature in Kelvin. The Arrhenius analysis is shown in Fig. 5b.  $\Delta H^\ddagger$  is the enthalpy associated with the melting of base pairs that must occur in order for the binary complex to nucleate. The data indicate that all retroviral NCs produce similar reductions in melting enthalpy relative to the no-NC reaction (Table 1). These results are consistent with the prediction that all retroviral NCs bind with more favorable enthalpy to single-stranded nucleic acids than to double-stranded nucleic acids.

(iii) **Equilibrium stability of the mini-TAR RNA/DNA duplex.** The annealing of mini-TAR RNA/DNA to form a complete duplex is driven by formation of nine new base pairs but is opposed by the entropy loss of one of the hairpins. Decreased stability of the annealed duplex, or lowering of the hairpin concentration, leads to a shift in equilibrium toward the reactants. In the absence of NC at long reaction times (i.e., hours or even days) (reference 104 and data not shown), equilibrium plateau levels of annealing are achieved that approach 100%. Therefore, the time courses for mini-TAR RNA/mini-TAR DNA annealing in the absence of NC are always fitted to equation 3, with  $P_\infty$  equal to 100. In contrast, in the presence of NC proteins, annealing remains incomplete at equilibrium due to NC-induced destabilization of the annealed duplex. In other words, NC proteins facilitate nucleic acid dissociation to

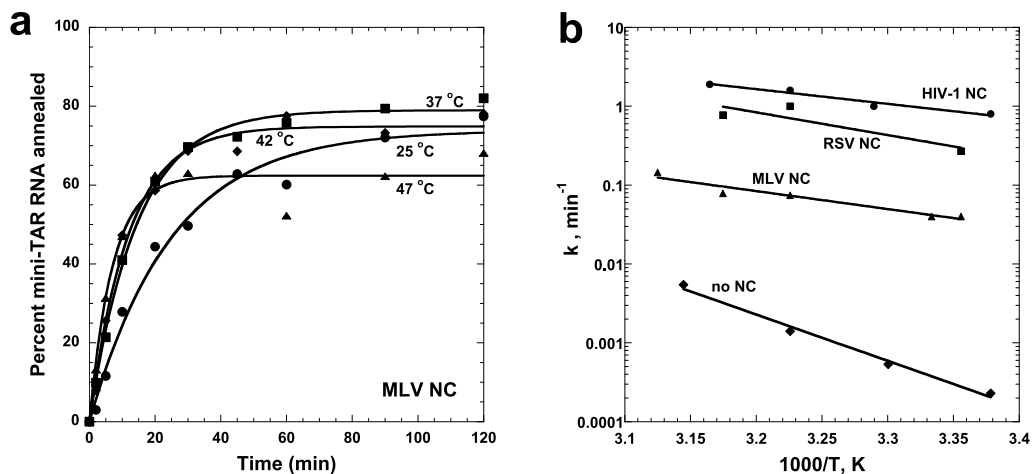


FIG. 5. Temperature dependence of mini-TAR RNA/DNA annealing kinetics. (a) Annealing time course of 15 nM mini-TAR RNA and 45 nM mini-TAR DNA in the presence of 3  $\mu$ M MLV NC at four different temperatures, as indicated in the figure. (b) Annealing rates plotted as a function of the reciprocal temperature in the absence and presence of 1.5  $\mu$ M HIV-1 NC (1.2 nt/NC), 1  $\mu$ M RSV NC (1.8 nt/NC), and 3  $\mu$ M MLV NC (0.6 nt/NC). The lines are the fits of the data points to the Arrhenius expression (equation 5) with slopes equal to the enthalpies of the rate-limiting step of annealing.

an even greater extent than annealing. Therefore, while the equilibrium in the presence of NC proteins is achieved much faster than in the absence of protein, the amount of product is smaller. In this case, the percentage of mini-TAR RNA annealed at equilibrium,  $P_\infty$ , can be used to estimate the free energy of annealing:

$$\Delta G = -RT \cdot \ln \left[ \frac{P_\infty}{100 - P_\infty} \right] = -RT \cdot \ln \left[ \frac{D}{K_d^{\text{mTAR}}} \right] \quad (6)$$

where  $K_d^{\text{mTAR}}$  is the dissociation constant of the fully annealed duplex.

The free-energy values for mini-TAR annealing calculated from measured  $P_\infty$  values according to equation 6 are presented in Fig. 6a as a function of  $D$ . The lines in the figure represent fits of these data using the second equality in equation 6 and  $K_d^{\text{mTAR}}$  as the fitting parameter. The  $K_d^{\text{mTAR}}$  values obtained suggest that the annealed duplex in the presence of the retroviral NCs is relatively stable, with the highest stability observed for RSV NC (Table 2). The theoretical  $\Delta G(D)$  dependence (i.e., the lines in Fig. 6a) describes the measured  $\Delta G(D)$  values (i.e., the symbols in Fig. 6a) quite well. This result supports the hypothesis that the change in equilibrium

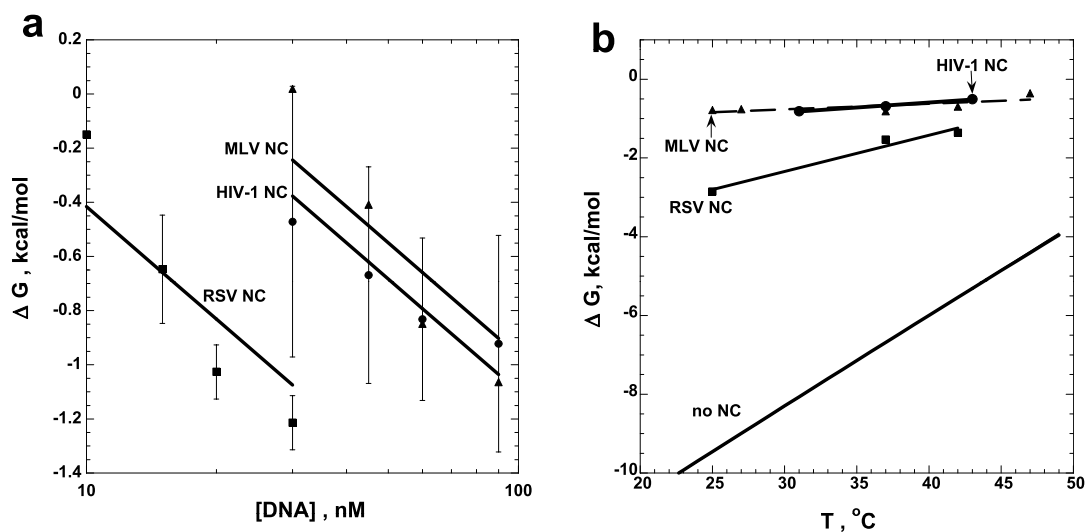


FIG. 6. Free energy of mini-TAR RNA/DNA hairpin annealing in the presence of HIV-1, RSV, and MLV NCs. The data points were calculated from the measured equilibrium annealing levels according to equation 6. Each data point is an average of at least three measurements. (a)  $D$  dependence of annealing free energy at 37 $^\circ$ C. The lines are  $\Delta G(D)$  dependencies calculated according to the second equality in equation 6, with  $K_d^{\text{mTAR}}$  as a fitting parameter. The fitted  $K_d^{\text{mTAR}}$  values are reported in Table 2. The error bars represent standard deviations. (b) Temperature dependence of annealing free energy. The lines are linear fits of the experimental data points to equation 7. The line for MLV NC is dashed. The free energy of annealing of mini-TAR RNA/DNA hairpins in the absence of NC was calculated for the given solution conditions using DINAMelt (72). The fitted values of  $\Delta H$  and  $\Delta S$ , along with  $\Delta G^{37}$ , are summarized in Table 2, where  $\Delta G^{37}$  is the annealing free energy at 37 $^\circ$ C.

TABLE 2. Thermodynamic parameters for annealing of mini-TAR RNA/DNA in the absence and presence of HIV-1, RSV, and MLV NCs

NC	$P_{\infty}$ (%) <sup>a</sup>	$\Delta G^{37}$ (kcal/mol) <sup>b</sup>	$K_d^{\text{mini-TAR}}$ (M) <sup>c</sup>	$\Delta H$ (kcal/mol) <sup>d</sup>	$\Delta S$ (kcal/mol) <sup>d</sup>
None	100	-6.7	$<10^{-9}$	-77.6	-232
HIV-1	$76 \pm 5$	$-0.7 \pm 2$	$(1.6 \pm 0.1) \times 10^{-8}$	$-8.5 \pm 4$	$-25 \pm 12$
RSV	$95 \pm 5$	$-1.5 \pm 2$	$(0.5 \pm 0.1) \times 10^{-8}$	$-14 \pm 8$	$-92 \pm 15$
MLV	$66 \pm 5$	$-0.8 \pm 2$	$(2.0 \pm 0.2) \times 10^{-8}$	$-5.2 \pm 3$	$-14 \pm 18$

<sup>a</sup>  $P_{\infty}$  is the equilibrium amount of 15 nM mini-TAR RNA annealed to 45 nM mini-TAR DNA in the absence or presence of saturating NC protein.

<sup>b</sup>  $\Delta G^{37}$  is the free energy of annealing under standard solution conditions of 15 nM mini-TAR RNA and 45 nM mini-TAR obtained from measured  $P_{\infty}$  according to equation 6.

<sup>c</sup>  $K_d^{\text{mini-TAR}}$  is the mini-TAR RNA/DNA duplex dissociation constant obtained by fitting the experimental  $D$  dependence of  $\Delta G^{37}$  to equation 6.

<sup>d</sup>  $\Delta H$  and  $\Delta S$  are the enthalpy and entropy of mini-TAR hairpin annealing obtained by fitting the measured temperature dependence of  $\Delta G^{37}$  to equation 7. The free energy, enthalpy, and entropy of mini-TAR DNA/DNA annealing in the absence of NC were calculated with DINAmelt (72).

annealing with  $D$  in the presence of NC is a result of changing stability of the annealed duplex. The accuracy of the  $\Delta G$  determination is not very high due to variability in measured  $P_{\infty}$  levels between individual assays. Nevertheless, the  $\Delta G$  values provide insights into the relative duplex-destabilizing abilities of HIV-1, RSV, and MLV NCs. The annealed mini-TAR duplex is most stable in the presence of RSV NC, suggesting that RSV NC does not destabilize nucleic acid base pairs as efficiently as HIV-1 NC. HIV-1 NC and MLV NC appear to be very similar in their duplex-destabilizing abilities.

The effects of the different NCs on the enthalpy,  $\Delta H$ , and entropy,  $\Delta S$ , of annealing were determined by measuring the equilibrium annealing levels,  $P_{\infty}$ , of mini-TAR as a function of temperature. The  $P_{\infty}$  values were used to calculate the annealing free energies,  $\Delta G$ , according to equation 6, and then  $\Delta G$  was fitted as a function of temperature to the general thermodynamic relationship:

$$\Delta G(T) = \Delta H - T \Delta S \quad (7)$$

The estimated  $\Delta G$  values, along with the fits to equation 7, are presented in Fig. 6b, and the resulting thermodynamic parameters are summarized in Table 2. As observed for HIV-1 NC, MLV NC strongly reduced the melting enthalpy and entropy of the annealed duplex. The effects of HIV-1 NC and MLV NC on the thermodynamic parameters of duplex melting were almost indistinguishable from each other within the accuracy of these measurements (Fig. 6b and Table 2). While RSV NC also significantly reduced the melting enthalpy, it had less of an effect on the melting entropy than HIV-1 or MLV NC. As discussed previously, the physical reason for the reduction in  $\Delta H$  and  $\Delta S$  in the presence of NC is likely due to the favorable enthalpy of NC interaction with single-stranded nucleic acids, which stabilizes the melted state, coupled with a loss of entropy upon NC binding to single-stranded nucleic acids (104). The combination of these two effects results in moderate duplex destabilization, since the protein's effect on the melting enthalpy is slightly stronger than its effect on the entropic component. Thus, the results obtained here suggest that RSV NC may not stabilize the melted state as effectively as HIV-1 NC and that RSV NC-bound single-stranded nucleic acids are more mobile in solution. In summary, analysis of the equilibrium mini-TAR RNA/DNA annealing levels in the presence of HIV, RSV, and MLV NCs suggests that the duplex-destabilizing abilities of NC proteins decrease in the following order: HIV  $\sim$  MLV  $>$  RSV.

**Effects of different retroviral NC proteins on mini-TAR RNA/DNA aggregation.** To directly examine the aggregation abilities of the four retroviral NCs, a sedimentation assay was used to measure the fraction of aggregated mini-TAR molecules as a function of the NC concentration under the same conditions used in the gel shift annealing assays (Fig. 7). The results suggest that all NC proteins, except for HTLV-1 NC, effectively aggregate nucleic acids upon saturated binding at  $\sim 1 \mu\text{M}$ . The results obtained for HIV-1 NC are consistent with previous findings (66, 98, 104). RSV NC appears to be slightly more effective at aggregating nucleic acids than HIV-1 NC, and these results are consistent with its ability to effectively facilitate the bimolecular-association step ( $k$  values in Table 1). MLV NC also exhibits good aggregation activity at concentrations of  $\geq 1 \mu\text{M}$ , despite the fact that this NC is significantly less effective at facilitating the bimolecular-association step than HIV-1 NC or RSV NC (compare the  $k$  values in Table 1). Interestingly, a previous study showed that the morphologies of nucleic acid aggregates formed in the presence of HIV-1 NC differ from those of MLV NC (77). Strikingly, HTLV-1 NC

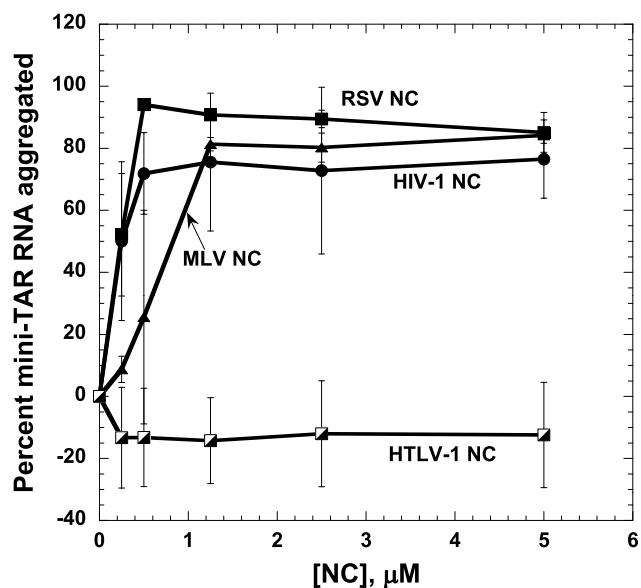


FIG. 7. Percents of mini-TAR RNA aggregated from a solution of 15 nM  $^{32}\text{P}$ -labeled mini-TAR RNA and 45 nM mini-TAR DNA at  $37^\circ\text{C}$  as a function of the NC concentration. The error bars represent standard deviations.

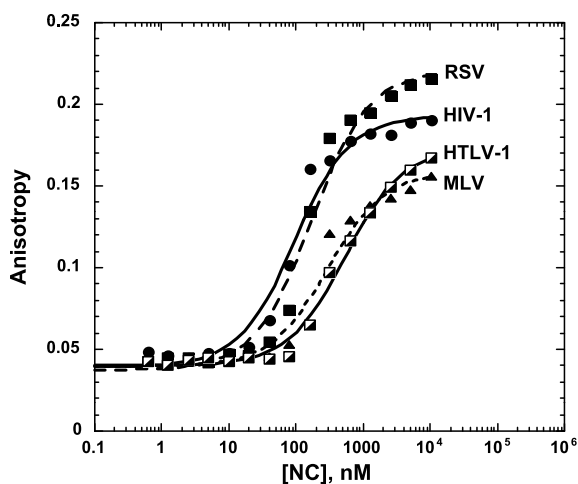


FIG. 8. FA binding analysis. Various concentrations of HIV-1, RSV, MLV, and HTLV-1 NCs were incubated with a 20-nt ssDNA, 5'-FAM-CTTCTTTGGGAGTGAATTAG-3'. The curves represent fits of the data to equation 1.

lacks any detectable nucleic-acid-aggregating activity in the range of concentrations studied (i.e., up to 5  $\mu$ M NC). In contrast to the other NC proteins, which are highly charged cationic proteins, HTLV-1 NC is neutral (pI,  $\sim$ 7) at physiological pH. The C-terminal domain of HTLV-1 NC contains a high density of acidic residues, whereas the majority of the basic residues are concentrated in the N terminus and zinc finger domains (Fig. 1a). Therefore, HTLV-1 NC's inability to aggregate nucleic acids is consistent with the electrostatic model of NC-induced nucleic acid aggregation (81, 92).

**Nucleic acid binding studies of different retroviral NC proteins.** FA was used to examine the binding of HIV-1, RSV, MLV, and HTLV-1 NCs to a 20-nt ssDNA oligonucleotide and a 20-bp double-stranded RNA/DNA (dsRNA/DNA) hybrid duplex (Fig. 8). The  $K_d$  values determined from these measurements are listed in Table 3. The  $K_d^{ss}$  and  $K_d^{ds}$  values for the NC proteins differ from each other by less than  $\sim$ 4-fold and  $\sim$ 7-fold, respectively. In addition, for each NC studied, the  $K_d^{ss}$  is two- to threefold smaller than  $K_d^{ds}$ , with the exception of HTLV-1 NC, where the difference is closer to fourfold. The binding strengths of the proteins decrease in the order HIV-1 NC > RSV NC > MLV NC > HTLV-1 NC for both the ssDNA and the dsRNA/DNA duplex. These binding measurements were carried out using a fairly random nucleic acid sequence in order to minimize sequence-specific binding effects. Although NCs generally bind nucleic acids nonspecifically, HIV-1 NC (2–4, 28, 40, 41, 105) and MLV NC (31, 35, 36) have an  $\sim$ 10-fold preference for single-stranded TG- or UG-rich sequences, and RSV NC has a preference for G residues (12, 31, 97, 105, 112, 113).

**Duplex destabilization by retroviral NC proteins.** Stronger binding to single-stranded versus double-stranded nucleic acids is characteristic of proteins that induce duplex destabilization (75). Assuming a similar site size of 6 nt (or 3 bp) (25, 32, 40, 41, 61, 62, 78, 100, 101, 105, 111) for binding to single-stranded and double-stranded sequences, the maximum duplex destabilization free energy by NC protein,  $\delta G$ , per base pair can be approximated according to equation 8 (75):

$$\delta G = \frac{2}{3} \cdot RT \cdot \ln \left[ \frac{K_d^{ss}}{K_d^{ds}} \right] \quad (8)$$

Values for the base pair destabilization free energies were calculated using equation 8, and the  $K_d^{ss}$  and  $K_d^{ds}$  values are given in Table 3. The destabilization free energy per base pair,  $\delta G$ , values for different retroviral NC proteins range between  $-0.3$  and  $-0.5$  kcal/mol/bp (Table 3). For HIV-1 NC, this estimate is consistent with other studies (when extrapolated to the present salt conditions) (7–9, 14, 23, 25, 57, 58, 101, 107, 110). To the best of our knowledge, there are no reported estimates of this quantity for the other retroviral NCs.

Interestingly, the NC-induced destabilization free energies calculated for the four retroviral NCs studied here are rather similar, with the  $\delta G$  value for HIV-1 NC at the lower end and that for HTLV-1 NC at the higher end of the range. The accuracy of  $\delta G$  is limited by errors in the  $K_d$  measurements. The FA curves obtained were fitted assuming a single binding site per oligonucleotide (see Materials and Methods), although it is likely that there are multiple NC binding sites, especially considering that 20-nt single-stranded and double-stranded sequences were used. Another source of uncertainty in  $\delta G$  is the assumption in equation 8 that the NC binding site sizes for single-stranded and double-stranded nucleic acids are the same. Nevertheless, these estimates of NC-induced duplex destabilization are generally consistent with the results of the annealing assays (Fig. 6). Due to its weak overall annealing activity, a detailed kinetic analysis of HTLV-1 NC could not be carried out using the gel shift assay, yet interestingly, this retroviral NC protein has the lowest  $\delta G$  value and is therefore expected to display stronger duplex destabilization activity than HIV-1 NC (Table 3). Ensemble and single-molecule fluorescence resonance energy transfer-based studies have been carried out to directly probe the destabilization activity of HTLV-1 NC, and the results are consistent with this hypothesis (M. Mitra, I. Rouzina, and K. Musier-Forsyth, unpublished observations; Q. Darugar, H. Kim, R. J. Gorelick, and C. Landes, unpublished data).

Taken together, the average duplex-destabilizing effect measured for all four retroviral NC proteins was as follows:  $\delta G =$

TABLE 3. Duplex destabilization free energies and apparent equilibrium dissociation constants for binding of retroviral NC proteins to single-stranded and double-stranded nucleic acids

NC	$K_d^{ss}$ (nM) (FA) <sup>a</sup>	$K_d^{ds}$ (nM) (FA) <sup>a</sup>	$\delta G$ (kcal/mol/bp) <sup>b</sup>	$K_d$ (nM) (DNA stretching) <sup>c</sup>
HIV-1	123 $\pm$ 9	233 $\pm$ 11	$-0.26 \pm 0.06$	10 $\pm$ 5
RSV	200 $\pm$ 49	660 $\pm$ 47	$-0.46 \pm 0.06$	80 $\pm$ 10
MLV	334 $\pm$ 34	1,092 $\pm$ 28	$-0.46 \pm 0.06$	150 $\pm$ 20
HTLV-1	431 $\pm$ 87	1,625 $\pm$ 270	$-0.52 \pm 0.06$	300 $\pm$ 50

<sup>a</sup>  $K_d^{ss}$  and  $K_d^{ds}$  are dissociation constants measured using FA for binding to an ssDNA 20-mer and a 20-bp RNA/DNA hybrid duplex, respectively.

<sup>b</sup>  $\delta G$  is the protein-induced destabilization per base pair, assuming that each protein is bound to 6 nt or 3 bp, estimated from the measured  $K_d^{ss}$  and  $K_d^{ds}$  values according to equation 8.

<sup>c</sup>  $K_d$  values determined from  $\lambda$ -DNA stretching are derived from protein titrations in solutions containing 50 mM NaCl (HIV-1, RSV, and MLV) or 6.2 mM NaCl (HTLV-1) as described in Materials and Methods. In these determinations, the  $K_d$  is an average value between ss- and dsDNA binding, with a larger contribution from ssDNA.

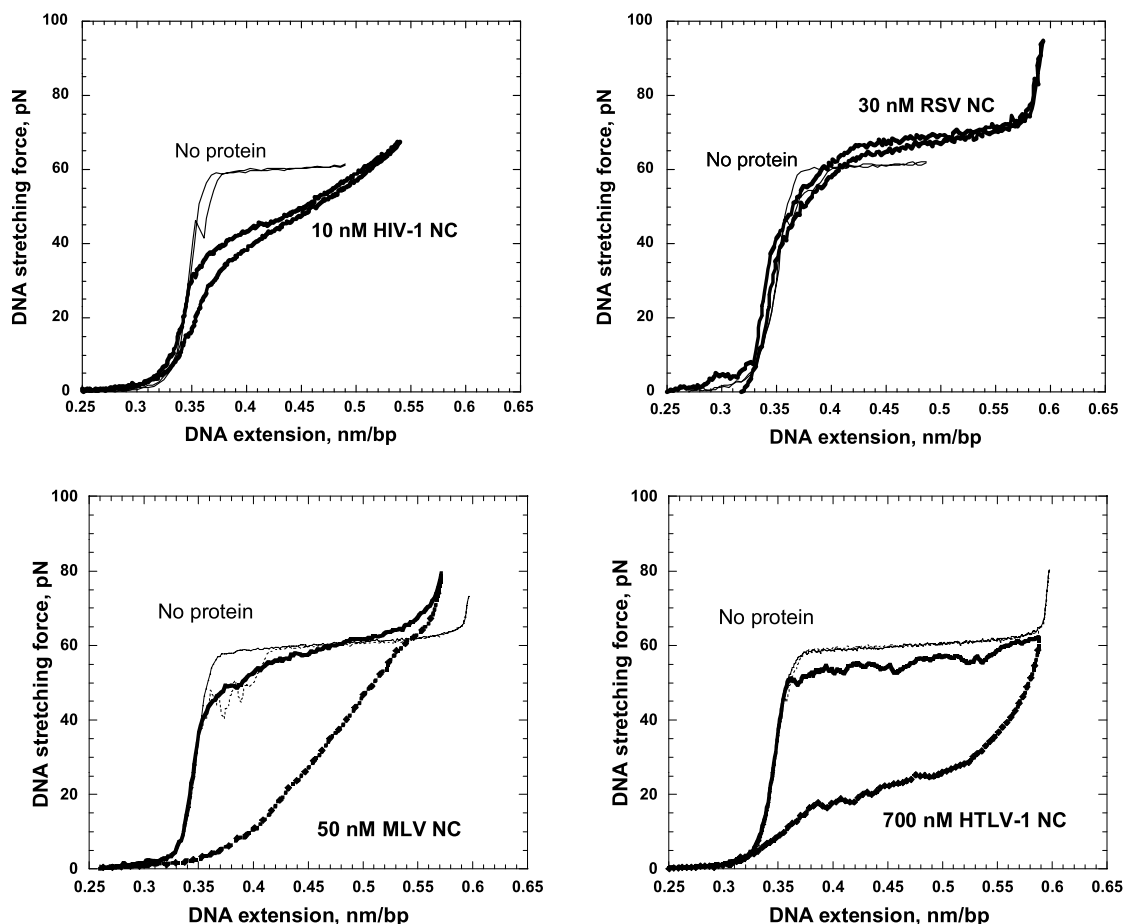


FIG. 9.  $\lambda$ -DNA stretching and relaxation curves in the presence of saturating levels of HIV-1 (top left), RSV (top right), MLV (bottom left), and HTLV-1 (bottom right) NCs. In each panel, the thin lines represent the curves in the absence of protein. Experiments in the presence of NC are shown by the thick black lines. The experiments were performed in 45 mM NaCl and 10 mM HEPES, pH 7.5, for a total of 50 mM Na<sup>+</sup>. In each cycle shown, the upper curve represents the stretching and the lower curve is the relaxation.

$-0.43 \pm 0.1$  kcal/mol/bp. This is a rather moderate effect, considering that the average melting free energy per base pair at 37°C is  $\sim 2$  kcal/mol/bp for DNA and  $\sim 3$  kcal/mol/bp for RNA duplexes (17, 95). However, it is sufficient to lead to the strong effects of some NC proteins on both the kinetics and equilibrium annealing levels of the TAR hairpins. The overall effect of a chaperone protein on duplex stability is expected to be similar to the effect of increasing the solution temperature according to equation 9:

$$\delta T = \delta G / \Delta S = (0.43 \text{ kcal/mol/bp}) / (0.025 \text{ kcal/mol/K/bp}) \approx 18^\circ\text{C} \quad (9)$$

where the entropy of melting,  $\Delta S$ , is assumed to be 0.025 kcal/mol/K/bp (56, 95). Thus, the addition of saturating NC has the same effect on duplex stability as heating the solution by  $\sim 18^\circ\text{C}$ , which is an alternative way to facilitate nucleic acid refolding without melting the final lowest energy state (106).

**DNA-stretching studies with different retroviral NC proteins.** The small differences in the duplex-destabilizing abilities of the four NC proteins cannot account for the marked differences in their chaperone activities (Fig. 2). In addition, with the exception of HTLV-1 NC, the NC proteins studied here

exhibited similar aggregation abilities. To gain further insights into the differences in the thermodynamics and kinetics of NC-nucleic acid interactions, we performed single-molecule DNA-stretching experiments (23–25, 74, 82–84, 93, 96, 103, 107–110). In these studies, double-stranded  $\lambda$ -DNA is tethered between two beads, and force is applied to stretch the DNA through the helix-coil transition. The effect of HIV-1 NC on the force-induced melting transition of  $\lambda$ -DNA has been extensively studied (23–25, 107, 110). Briefly, binding of HIV-1 NC results in significant broadening of the melting transition (compared to the DNA-only curve, which displays a sharp plateau at  $\sim 60$  pN) and a reduction in the force required to stretch  $\lambda$ -DNA (Fig. 9a). The small hysteresis, that is, the lack of an exact match between the stretching and relaxation curves, is a sign of the fast kinetics of HIV-1 NC binding and dissociation to ds- and ssDNA on the time scale of the experiment. The high reproducibility of the stretching curves with repeated cycles and various pulling rates is indicative of an equilibrium process in which HIV-1 NC is able to rapidly adjust to changes in DNA structure (23).

The DNA stretching curves in the absence and presence of saturating amounts of each of the four NC proteins examined

here are presented in Fig. 9. RSV NC binding results in a dsDNA melting transition that remains highly cooperative and occurs at a force that exceeds the melting force measured in the absence of protein by  $\sim 5$  pN (Fig. 9b). A possible mechanism for this apparent duplex stabilization may involve changes in the elastic properties of ssDNA upon RSV NC binding. Similar to HIV-1 NC, RSV NC produces little hysteresis in the stretching cycle upon saturated DNA binding. In addition, RSV NC also produces a small but reproducible increase in the force at DNA extensions below the  $\lambda$ -DNA contour length (0.34 nm/bp). These two features signify fast kinetics of protein-DNA interaction and the ability to very effectively aggregate DNA, respectively, and are consistent with RSV NC's efficient facilitation of mini-TAR RNA/DNA annealing (Table 1 and Fig. 4 and 7).

Saturation with MLV NC results in broadening of the DNA melting transition and a large hysteresis that increases at higher NC concentrations (Fig. 9c). This large hysteresis indicates slow reannealing of the DNA strands after the release of tension. MLV NC destabilizes duplexes (Fig. 6 and Table 1) and aggregates nucleic acids quite efficiently (Fig. 7). Based on the results of the DNA-stretching assay, the reduced chaperone activity of MLV NC appears to be due to the relatively slow kinetics of MLV NC dissociation from single-stranded nucleic acids, which would be expected to inhibit duplex-closing events.

The effect of HTLV-1 NC on the DNA-stretching profile differs considerably from those of HIV-1, RSV, and MLV NCs (Fig. 9d). HTLV-1 NC has little effect on the transition width but reduces the force required for DNA melting. Strikingly, the HTLV-1 NC-stretching curve exhibits the greatest amount of hysteresis observed for any NC we have studied. This result implies that HTLV-1 NC preferentially binds ssDNA and, once bound, dissociates slowly, thereby completely preventing strand reannealing on the time scale of the experiment. The features of the HTLV-1 NC DNA stretching and relaxation curves are very similar to the DNA-stretching behavior in the presence of ssDNA binding proteins (SSBs), such as bacteriophage T4 gene 32 protein (gp32) (82–84, 93) and bacteriophage T7 gene 2.5 protein (gp2.5) (96). DNA-stretching studies have demonstrated that SSBs bind dsDNA very poorly and dissociate from ssDNA very slowly (82–84, 93, 96). In the case of gp32, its slow dissociation is due to the cooperativity of protein binding to ssDNA resulting from “head-to-tail” protein-protein interactions (83). In the case of HTLV-1 NC, it is plausible that the bound proteins interact in a similar fashion, with the cationic N-terminal domain of one NC binding to the anionic C-terminal domain of an adjacent NC molecule. Previously, fluorescence studies demonstrated that HTLV-1 NC binds nucleic acids with modest cooperativity (78). Such binding cooperativity might explain the slow dissociation of HTLV-1 NC from ssDNA. Taken together, these data suggest that the SSB-type properties of HTLV-1 NC are responsible for its poor performance as a nucleic acid chaperone.

DNA-stretching results were also used to estimate equilibrium dissociation constants (Table 3, column 5). These values are determined by measuring the slope of the linear region of the force transition width as a function of the concentration (equation 2) (see Materials and Methods) (23, 25, 73) and reflect a composite of affinities of binding to ssDNA and

dsDNA. When the protein binds ssDNA more strongly than dsDNA, the  $K_d$  values primarily reflect protein interactions with ssDNA. In accordance with the preference of all retroviral NCs for binding to ssDNA, the  $K_d$  values obtained from the stretching curves are more closely correlated with the values measured by FA analysis for single-stranded binding (Table 3, column 2) than for double-stranded binding (column 3). Interestingly, although the absolute values differ, the relative trends in strengths of binding to polymeric  $\lambda$ -DNA between the NC proteins is similar to the relative affinities measured for binding to a 20-nt ssDNA oligonucleotide (i.e., HIV-1 > RSV > MLV > HTLV-1 NC).

## DISCUSSION

In this work, the chaperone activities of HIV-1, RSV, MLV, and HTLV-1 NCs were characterized using complementary experimental approaches. Gel shift annealing assays demonstrated that the overall chaperone activities of the NC proteins studied decrease in the order HIV-1 NC  $\sim$  RSV NC > MLV NC  $\gg$  HTLV-1 NC (Fig. 2). Furthermore, detailed analysis of hairpin-annealing time courses as a function of the DNA concentration and temperature provide additional insights into how NC proteins differ in their nucleic acid chaperone activities. RSV NC effectively facilitates the bimolecular-association step of mini-TAR RNA/DNA annealing, suggesting that it is a better aggregating agent than HIV-1 NC. Overall, MLV NC is less efficient in facilitating both bimolecular association and conversion to the extended duplex. Thermodynamic analysis suggests that HIV-1 and MLV NCs are similar to each other and only slightly better than RSV NC at duplex destabilization, while all three reduce the melting enthalpy and entropy of the duplex.

Sedimentation assays demonstrated that HIV-1, RSV, and MLV NCs efficiently aggregate nucleic acids under saturating conditions ( $>1$   $\mu$ M protein), whereas HTLV-1 NC lacks nucleic-acid-aggregating capability. We hypothesize that HTLV-1 NC is unable to aggregate nucleic acids due to its overall neutral charge. Experiments in our laboratory have demonstrated that removal of the C-terminal cationic domain of HTLV-1 NC restores aggregation and chaperone activity (K. Stewart-Maynard, I. Rouzina, and K. Musier-Forsyth, unpublished data). Furthermore, measurements of equilibrium binding of the four NC proteins to 20-nt ssDNA and a dsRNA/DNA hybrid duplex suggest that the duplex-destabilizing abilities of the NC proteins studied here are similar. Interestingly, despite its poor overall chaperone activity, HTLV-1 NC appears to be a very effective duplex-destabilizing agent.

The observed differences in duplex destabilization and nucleic acid aggregation cannot fully account for the differences in nucleic acid chaperone activities between the four retroviral NC proteins. For instance, saturating concentrations of MLV NC aggregate nucleic acids as effectively as HIV-1 and RSV NC, and MLV's duplex destabilization capability is also similar to those of HIV-1 and RSV NCs. However, gel shift assays demonstrated that MLV NC does not facilitate mini-TAR RNA/DNA annealing as efficiently as HIV-1 or RSV NC. The rates of protein dissociation from ssDNA, revealed by single-molecule DNA-stretching experiments, decrease in the order RSV NC  $\geq$  HIV-1 NC  $\gg$  MLV NC  $\gg$  HTLV-1 NC,

which closely parallels their chaperone activities (Fig. 2). These results support the notion that the fast kinetics of protein-nucleic acid interaction is another major component of the NC nucleic acid chaperone function (23).

NC's ATP-independent chaperone function requires stoichiometric binding to facilitate nucleic acid aggregation and maximal duplex destabilization (104). High-affinity binding, in combination with fast kinetics, is a feature of cationic binding to nucleic acids in a predominately electrostatic mode (5, 16, 49, 50, 63, 71, 88, 90, 91). Such electrostatic binding leads to the formation of protein-induced nucleic acid aggregates that are characterized by high mobility of nucleic acid and protein (5, 15, 16, 50, 63, 80, 87, 92, 94, 102), thereby strongly facilitating the bimolecular steps of nucleic acid annealing. However, purely electrostatic binding results in stabilization of the double-stranded, rather than the single-stranded, form of nucleic acids (17), whereas duplex destabilization requires preferential binding to the single-stranded form. For HIV-1 NC, destabilization is facilitated, in part, by partial stacking of two conserved aromatic residues within the zinc finger domains (Fig. 1a) with nucleic acid bases (2–4, 28). RSV (112, 113) and MLV (31, 34) NC proteins also engage in similar interactions. While this binding leads to duplex destabilization, it is also expected to result in reduced dissociation kinetics. HIV-1 NC appears to have optimized these contradictory properties; it is a moderate duplex destabilizer, displaying rapid nucleic acid interaction kinetics and high aggregating ability. RSV NC is an even better aggregating agent and exhibits rapid binding kinetics, but it appears to be a relatively poor duplex destabilizer (Fig. 6, 7, and 9 and Table 1). MLV NC aggregates and destabilizes duplexes effectively (Fig. 6). However, due to its slow dissociation kinetics (Fig. 9), the protein is a less effective chaperone (Fig. 2). Recent studies support the conclusion that MLV NC is a less effective annealing agent than HIV-1 NC, despite the fact that it has similar binding and destabilization capabilities (37). MLV NC was also shown to reduce the rate of HIV-1 reverse transcription (76) and to induce DNA aggregates of lower density than HIV-1 NC (77).

The chaperone properties of HTLV-1 NC differ substantially from those of the other retroviral NCs. Despite the fact that this deltaretroviral NC is a relatively strong duplex destabilizer, the neutral protein does not cause nucleic acid aggregation. Our DNA-stretching data suggest that HTLV-1 NC's extremely slow nucleic acid dissociation kinetics is likely the major factor leading to the poor chaperone properties observed *in vitro* (Fig. 2). The implications of these findings for RNA packaging and reverse transcription *in vivo* remain to be explored, and additional studies using HTLV-1 NC protein variants are currently under way.

In this work, we have investigated the effects of different retroviral NC proteins on a reaction that models the TAR RNA/DNA annealing that occurs during the minus-strand transfer step of HIV-1 reverse transcription. However, the R regions of the four retroviruses differ in length, sequence, and structural stability. For example, the R region of RSV is only 21 nt long and lacks significant secondary structure (1). Therefore, one can speculate that the somewhat weaker duplex-destabilizing ability of RSV NC coevolved with the unstructured R region of the retrovirus. The 68-nt R region of MLV is comparable in length to the 98-nt R region of HIV-1 and

folds into several hairpins with stability comparable to that of HIV-1 TAR. This observation is consistent with the similar duplex-destabilizing capabilities of these NC proteins.

Given the poor chaperone activity of HTLV-1 NC relative to the other retroviral NCs examined here, it is surprising that the HTLV-1 R region contains 228 nt and folds into a complex secondary structure (6). The chaperone function of HTLV-1 NC may be regulated by other factors *in vivo*, possibly involving a conformational change of the protein's unique acidic C-terminal domain. Alternatively, other host or viral proteins may be involved in chaperoning key steps in reverse transcription in this retrovirus. Clearly, additional studies of the chaperone activities of different NC proteins using substrates that mimic their respective R regions are needed to better understand the biological roles of the observed differences in chaperone properties.

#### ACKNOWLEDGMENTS

We thank Cathy V. Hixson and Donald G. Johnson for their assistance in preparing the recombinant NC proteins.

This work was supported by NIH grants GM065056 (to K.M.-F.) and GM073462 (to M.C.W.), by NSF grant MCB-0744456 (to M.C.W.), and by an NIH Ruth L. Kirschstein National Service Award GM072396 (to K.M.S.-M.). This publication was funded in part with federal funds from the National Cancer Institute, National Institutes of Health, under contract N01-CO-12400.

The content of this publication does not necessarily reflect the views or policies of the Department of Health and Human Services, nor does mention of trade names, commercial products, or organizations imply endorsement by the U.S. government.

#### REFERENCES

- Allain, B., J. B. Rascle, H. de Rocquigny, B. Roques, and J. L. Darlix. 1998. *cis* elements and *trans*-acting factors required for minus strand DNA transfer during reverse transcription of the genomic RNA of murine leukemia virus. *J. Mol. Biol.* **277**:225–235.
- Amarasinghe, G. K., R. N. De Guzman, R. B. Turner, K. J. Chancellor, Z. R. Wu, and M. F. Summers. 2000. NMR structure of the HIV-1 nucleocapsid protein bound to stem-loop SL2 of the psi-RNA packaging signal. Implications for genome recognition. *J. Mol. Biol.* **301**:491–511.
- Amarasinghe, G. K., R. N. De Guzman, R. B. Turner, and M. F. Summers. 2000. NMR structure of stem-loop SL2 of the HIV-1 psi RNA packaging signal reveals a novel A-U-A base-triple platform. *J. Mol. Biol.* **299**:145–156.
- Amarasinghe, G. K., J. Zhou, M. Miskimon, K. J. Chancellor, J. A. McDonald, A. G. Matthews, R. R. Miller, M. D. Rouse, and M. F. Summers. 2001. Stem-loop SL4 of the HIV-1 psi RNA packaging signal exhibits weak affinity for the nucleocapsid protein. Structural studies and implications for genome recognition. *J. Mol. Biol.* **314**:961–970.
- Arscott, P. G., C. Ma, J. R. Wenner, and V. A. Bloomfield. 1995. DNA condensation by cobalt hexammine (III) in alcohol-water mixtures: dielectric constant and other solvent effects. *Biopolymers* **36**:345–364.
- Askjaer, P., and J. Kjems. 1998. Mapping of multiple RNA binding sites of human T-cell lymphotropic virus type I Rex protein within 5'- and 3'-Rex response elements. *J. Biol. Chem.* **273**:11463–11471.
- Azoulay, J., J. P. Clamme, J. L. Darlix, B. P. Roques, and Y. Mély. 2003. Destabilization of the HIV-1 complementary sequence of TAR by the nucleocapsid protein through activation of conformational fluctuations. *J. Mol. Biol.* **326**:691–700.
- Beltz, H., J. Azoulay, S. Bernacchi, J. P. Clamme, D. Ficheux, B. Roques, J. L. Darlix, and Y. Mély. 2003. Impact of the terminal bulges of HIV-1 cTAR DNA on its stability and the destabilizing activity of the nucleocapsid protein NCp7. *J. Mol. Biol.* **328**:95–108.
- Beltz, H., C. Clauss, E. Piemont, D. Ficheux, R. J. Gorelick, B. Roques, C. Gabus, J. L. Darlix, H. de Rocquigny, and Y. Mély. 2005. Structural determinants of HIV-1 nucleocapsid protein for cTAR DNA binding and destabilization, and correlation with inhibition of self-primed DNA synthesis. *J. Mol. Biol.* **348**:1113–1126.
- Beltz, H., E. Piemont, E. Schaub, D. Ficheux, B. Roques, J. L. Darlix, and Y. Mély. 2004. Role of the structure of the top half of HIV-1 cTAR DNA on the nucleic acid destabilizing activity of the nucleocapsid protein NCp7. *J. Mol. Biol.* **338**:711–723.
- Berg, J. M. 1986. Potential metal-binding domains in nucleic acid binding proteins. *Science* **232**:485–487.

12. Berglund, J. A., B. Charpentier, and M. Rosbash. 1997. A high affinity binding site for the HIV-1 nucleocapsid protein. *Nucleic Acids Res.* **25**: 1042–1049.
13. Berkowitz, R., J. Fisher, and S. P. Goff. 1996. RNA packaging. *Curr. Top. Microbiol. Immunol.* **214**:177–218.
14. Bernacchi, S., S. Stoylov, E. Piemont, D. Ficheux, B. P. Roques, J. L. Darlix, and Y. Mély. 2002. HIV-1 nucleocapsid protein activates transient melting of least stable parts of the secondary structure of TAR and its complementary sequence. *J. Mol. Biol.* **317**:385–399.
15. Besteman, K., M. A. Zevenbergen, and S. G. Lemay. 2005. Charge inversion by multivalent ions: dependence on dielectric constant and surface-charge density. *Phys. Rev. E* **72**:061501.
16. Bloomfield, V. A. 1997. DNA condensation by multivalent cations. *Biopolymers* **44**:269–282.
17. Bloomfield, V. A., D. M. Crothers, and I. Tinoco. 2000. *Nucleic acids structure, properties, and function.* University Science Books, Sausalito, CA.
18. Brulé, F., G. Bec, G. Keith, S. F. Le Grice, B. P. Roques, B. Ehresmann, C. Ehresmann, and R. Marquet. 2000. In vitro evidence for the interaction of tRNA(3)(Lys) with U3 during the first strand transfer of HIV-1 reverse transcription. *Nucleic Acids Res.* **28**:634–640.
19. Carreau, S., R. J. Gorelick, and F. D. Bushman. 1999. Coupled integration of human immunodeficiency virus type 1 cDNA ends by purified integrase in vitro: stimulation by the viral nucleocapsid protein. *J. Virol.* **73**:6670–6679.
20. Chan, B., and K. Musier-Forsyth. 1997. The nucleocapsid protein specifically anneals tRNA<sup>Lys</sup>-3 onto a noncomplementary primer binding site within the HIV-1 RNA genome in vitro. *Proc. Natl. Acad. Sci. USA* **94**: 13530–13535.
21. Chan, B., K. Weidemaier, W. T. Yip, P. F. Barbara, and K. Musier-Forsyth. 1999. Intra-tRNA distance measurements for nucleocapsid protein-dependent tRNA unwinding during priming of HIV reverse transcription. *Proc. Natl. Acad. Sci. USA* **96**:459–464.
22. Cristofari, G., and J. L. Darlix. 2002. The ubiquitous nature of RNA chaperone proteins. *Prog. Nucleic. Acid Res. Mol. Biol.* **72**:223–268.
23. Cruceanu, M., R. J. Gorelick, K. Musier-Forsyth, I. Rouzina, and M. C. Williams. 2006. Rapid kinetics of protein-nucleic acid interaction is a major component of HIV-1 nucleocapsid protein's nucleic acid chaperone function. *J. Mol. Biol.* **363**:867–877.
24. Cruceanu, M., A. G. Stephen, P. J. Beuning, R. J. Gorelick, R. J. Fisher, and M. C. Williams. 2006. Single DNA molecule stretching measures the activity of chemicals that target the HIV-1 nucleocapsid protein. *Anal. Biochem.* **358**:159–170.
25. Cruceanu, M., M. A. Urbaneja, C. V. Hixson, D. G. Johnson, S. A. Datta, M. J. Fivash, A. G. Stephen, R. J. Fisher, R. J. Gorelick, J. R. Casas-Finet, A. Rein, I. Rouzina, and M. C. Williams. 2006. Nucleic acid binding and chaperone properties of HIV-1 Gag and nucleocapsid proteins. *Nucleic Acids Res.* **34**:593–605.
26. Darlix, J. L., C. Gabus, M. T. Nugeyre, F. Clavel, and F. Barre-Sinoussi. 1990. *cis* elements and *trans*-acting factors involved in the RNA dimerization of the human immunodeficiency virus HIV-1. *J. Mol. Biol.* **216**:689–699.
27. Darlix, J. L., M. Lapadat-Tapolsky, H. de Rocquigny, and B. P. Roques. 1995. First glimpses at structure-function relationships of the nucleocapsid protein of retroviruses. *J. Mol. Biol.* **254**:523–537.
28. De Guzman, R. N., Z. R. Wu, C. C. Stalling, L. Pappalardo, P. N. Borer, and M. F. Summers. 1998. Structure of the HIV-1 nucleocapsid protein bound to the SL3 psi-RNA recognition element. *Science* **279**:384–388.
29. De Rocquigny, H., C. Gabus, A. Vincent, M. C. Fournie-Zaluski, B. Roques, and J. L. Darlix. 1992. Viral RNA annealing activities of human immunodeficiency virus type 1 nucleocapsid protein require only peptide domains outside the zinc fingers. *Proc. Natl. Acad. Sci. USA* **89**:6472–6476.
30. Derse, D., J. Mikovits, M. Polianova, B. K. Felber, and F. Ruscetti. 1995. Virions released from cells transfected with a molecular clone of human T-cell leukemia virus type I give rise to primary and secondary infections of T cells. *J. Virol.* **69**:1907–1912.
31. Dey, A., D. York, A. Smalls-Mantey, and M. F. Summers. 2005. Composition and sequence-dependent binding of RNA to the nucleocapsid protein of Moloney murine leukemia virus. *Biochemistry* **44**:3735–3744.
32. Dib-Hajj, F., R. Khan, and D. P. Giedroc. 1993. Retroviral nucleocapsid proteins possess potent nucleic acid strand renaturation activity. *Protein Sci.* **2**:231–243.
33. Driscoll, M. D., and S. H. Hughes. 2000. Human immunodeficiency virus type 1 nucleocapsid protein can prevent self-priming of minus-strand stop DNA by promoting the annealing of short oligonucleotides to hairpin sequences. *J. Virol.* **74**:8785–8792.
34. D'Souza, V., A. Dey, D. Habib, and M. F. Summers. 2004. NMR structure of the 101-nucleotide core encapsidation signal of the Moloney murine leukemia virus. *J. Mol. Biol.* **337**:427–442.
35. D'Souza, V., J. Melamed, D. Habib, K. Pullen, K. Wallace, and M. F. Summers. 2001. Identification of a high affinity nucleocapsid protein binding element within the Moloney murine leukemia virus Psi-RNA packaging signal: implications for genome recognition. *J. Mol. Biol.* **314**:217–232.
36. D'Souza, V., and M. F. Summers. 2004. Structural basis for packaging the dimeric genome of Moloney murine leukaemia virus. *Nature* **431**:586–590.
37. Egele, C., E. Piemont, P. Didier, D. Ficheux, B. Roques, J. L. Darlix, H. de Rocquigny, and Y. Mély. 2007. The single-finger nucleocapsid protein of Moloney murine leukemia virus binds and destabilizes the TAR sequences of HIV-1 but does not promote efficiently their annealing. *Biochemistry* **46**:14650–14662.
38. Feng, Y. X., S. Campbell, D. Harvin, B. Ehresmann, C. Ehresmann, and A. Rein. 1999. The human immunodeficiency virus type 1 Gag polyprotein has nucleic acid chaperone activity: possible role in dimerization of genomic RNA and placement of tRNA on the primer binding site. *J. Virol.* **73**:4251–4256.
39. Feng, Y. X., T. D. Copeland, L. E. Henderson, R. J. Gorelick, W. J. Bosche, J. G. Levin, and A. Rein. 1996. HIV-1 nucleocapsid protein induces "maturation" of dimeric retroviral RNA in vitro. *Proc. Natl. Acad. Sci. USA* **93**:7577–7581.
40. Fisher, R. J., M. J. Fivash, A. G. Stephen, N. A. Hagan, S. R. Shenoy, M. V. Medaglia, L. R. Smith, K. M. Worthy, J. T. Simpson, R. Shoemaker, K. L. McNitt, D. G. Johnson, C. V. Hixson, R. J. Gorelick, D. Fabris, L. E. Henderson, and A. Rein. 2006. Complex interactions of HIV-1 nucleocapsid protein with oligonucleotides. *Nucleic Acids Res.* **34**:472–484.
41. Fisher, R. J., A. Rein, M. Fivash, M. A. Urbaneja, J. R. Casas-Finet, M. Medaglia, and L. E. Henderson. 1998. Sequence-specific binding of human immunodeficiency virus type 1 nucleocapsid protein to short oligonucleotides. *J. Virol.* **72**:1902–1909.
42. Fu, W., R. J. Gorelick, and A. Rein. 1994. Characterization of human immunodeficiency virus type 1 dimeric RNA from wild-type and protease-defective virions. *J. Virol.* **68**:5013–5018.
43. Gao, K., R. J. Gorelick, D. G. Johnson, and F. Bushman. 2003. Cofactors for human immunodeficiency virus type 1 cDNA integration in vitro. *J. Virol.* **77**:1598–1603.
44. Green, L. M., and J. M. Berg. 1990. Retroviral nucleocapsid protein-metal ion interactions: folding and sequence variants. *Proc. Natl. Acad. Sci. USA* **87**:6403–6407.
45. Guo, J., L. E. Henderson, J. Bess, B. Kane, and J. G. Levin. 1997. Human immunodeficiency virus type 1 nucleocapsid protein promotes efficient strand transfer and specific viral DNA synthesis by inhibiting TAR-dependent self-priming from minus-strand strong-stop DNA. *J. Virol.* **71**:5178–5188.
46. Guo, J., T. Wu, J. Anderson, B. F. Kane, D. G. Johnson, R. J. Gorelick, L. E. Henderson, and J. G. Levin. 2000. Zinc finger structures in the human immunodeficiency virus type 1 nucleocapsid protein facilitate efficient minus- and plus-strand transfer. *J. Virol.* **74**:8980–8988.
47. Hargittai, M. R., R. J. Gorelick, I. Rouzina, and K. Musier-Forsyth. 2004. Mechanistic insights into the kinetics of HIV-1 nucleocapsid protein-facilitated tRNA annealing to the primer binding site. *J. Mol. Biol.* **337**:951–968.
48. Hargittai, M. R., A. T. Mangla, R. J. Gorelick, and K. Musier-Forsyth. 2001. HIV-1 nucleocapsid protein zinc finger structures induce tRNA(Lys,3) structural changes but are not critical for primer/template annealing. *J. Mol. Biol.* **312**:985–997.
49. He, S., P. G. Arscott, and V. A. Bloomfield. 2000. Condensation of DNA by multivalent cations: experimental studies of condensation kinetics. *Biopolymers* **53**:329–341.
50. Heilman-Miller, S. L., J. Pan, D. Thirumalai, and S. A. Woodson. 2001. Role of counterion condensation in folding of the Tetrahymena ribozyme. II. Counterion-dependence of folding kinetics. *J. Mol. Biol.* **309**:57–68.
51. Heilman-Miller, S. L., T. Wu, and J. G. Levin. 2004. Alteration of nucleic acid structure and stability modulates the efficiency of minus-strand transfer mediated by the HIV-1 nucleocapsid protein. *J. Biol. Chem.* **279**:44154–44165.
52. Henderson, L. E., T. D. Copeland, R. C. Sowder, G. W. Smythers, and S. Oroszlan. 1981. Primary structure of the low molecular weight nucleic acid-binding proteins of murine leukemia viruses. *J. Biol. Chem.* **256**:8400–8406.
53. Herschlag, D. 1995. RNA chaperones and the RNA folding problem. *J. Biol. Chem.* **270**:20871–20874.
54. Hong, M. K., E. J. Harbron, D. B. O'Connor, J. Guo, P. F. Barbara, J. G. Levin, and K. Musier-Forsyth. 2003. Nucleic acid conformational changes essential for HIV-1 nucleocapsid protein-mediated inhibition of self-priming in minus-strand transfer. *J. Mol. Biol.* **325**:1–10.
55. Hughes, S. H., J. J. Greenhouse, C. J. Petropoulos, and P. Suttrave. 1987. Adaptor plasmids simplify the insertion of foreign DNA into helper-independent retroviral vectors. *J. Virol.* **61**:3004–3012.
56. Jaeger, J. A., J. Santa Lucia, Jr., and I. Tinoco, Jr. 1993. Determination of RNA structure and thermodynamics. *Annu. Rev. Biochem.* **62**:255–287.
57. Kanevsky, I., F. Chaminade, D. Ficheux, A. Moumen, R. Gorelick, M. Negroni, J. L. Darlix, and P. Fosse. 2005. Specific interactions between HIV-1 nucleocapsid protein and the TAR element. *J. Mol. Biol.* **348**:1059–1077.
58. Kankia, B. I., G. Barany, and K. Musier-Forsyth. 2005. Unfolding of DNA quadruplexes induced by HIV-1 nucleocapsid protein. *Nucleic Acids Res.* **33**:4395–4403.

59. **Kapust, R. B., J. Tozser, T. D. Copeland, and D. S. Waugh.** 2002. The P1' specificity of tobacco etch virus protease. *Biochem. Biophys. Res. Commun.* **294**:949–955.
60. **Kapust, R. B., J. Tozser, J. D. Fox, D. E. Anderson, S. Cherry, T. D. Copeland, and D. S. Waugh.** 2001. Tobacco etch virus protease: mechanism of autolysis and rational design of stable mutants with wild-type catalytic proficiency. *Protein Eng.* **14**:993–1000.
61. **Karpel, R. L., L. E. Henderson, and S. Oroszlan.** 1987. Interactions of retroviral structural proteins with single-stranded nucleic acids. *J. Biol. Chem.* **262**:4961–4967.
62. **Khan, R., and D. P. Giedroc.** 1994. Nucleic acid binding properties of recombinant Zn2 HIV-1 nucleocapsid protein are modulated by COOH-terminal processing. *J. Biol. Chem.* **269**:22538–22546.
63. **Koculi, E., N. K. Lee, D. Thirumalai, and S. A. Woodson.** 2004. Folding of the Tetrahymena ribozyme by polyamines: importance of counterion valence and size. *J. Mol. Biol.* **341**:27–36.
64. **Lakowicz, J. R.** 1999. Principles of fluorescence spectroscopy, 2nd ed. Kluwer Academic, New York, NY.
65. **Lapadat-Tapolsky, M., C. Gabus, M. Rau, and J. L. Darlix.** 1997. Possible roles of HIV-1 nucleocapsid protein in the specificity of proviral DNA synthesis and in its variability. *J. Mol. Biol.* **268**:250–260.
66. **Le Cam, E., D. Coulaud, E. Delain, P. Petitjean, B. P. Roques, D. Gerard, E. Stoylova, C. Vuilleumier, S. P. Stoylov, and Y. Mély.** 1998. Properties and growth mechanism of the ordered aggregation of a model RNA by the HIV-1 nucleocapsid protein: an electron microscopy investigation. *Biopolymers* **45**:217–229.
67. **Levin, J. G., J. Guo, I. Rouzina, and K. Musier-Forsyth.** 2005. Nucleic acid chaperone activity of HIV-1 nucleocapsid protein: critical role in reverse transcription and molecular mechanism. *Prog. Nucleic Acid Res. Mol. Biol.* **80**:217–286.
68. **Li, X., Y. Quan, E. J. Arts, Z. Li, B. D. Preston, H. de Rocquigny, B. P. Roques, J. L. Darlix, L. Kleiman, M. A. Parniak, and M. A. Wainberg.** 1996. Human immunodeficiency virus type 1 nucleocapsid protein (NCp7) directs specific initiation of minus-strand DNA synthesis primed by human tRNA<sup>Lys3</sup> in vitro: studies of viral RNA molecules mutated in regions that flank the primer binding site. *J. Virol.* **70**:4996–5004.
69. **Liu, H. W., G. Cosa, C. F. Landes, Y. Zeng, B. J. Kovalski, D. G. Mullen, G. Barany, K. Musier-Forsyth, and P. F. Barbara.** 2005. Single-molecule FRET studies of important intermediates in the nucleocapsid-protein-chaperoned minus-strand transfer step in HIV-1 reverse transcription. *Biophys. J.* **89**:3470–3479.
70. **Lundblad, J. R., M. Laurance, and R. H. Goodman.** 1996. Fluorescence polarization analysis of protein-DNA and protein-protein interactions. *Mol. Endocrinol.* **10**:607–612.
71. **Manning, G. S.** 1978. The molecular theory of polyelectrolyte solutions with applications to the electrostatic properties of polynucleotides. *Q. Rev. Biophys.* **11**:179–246.
72. **Markham, N. R., and M. Zuker.** 2005. DINAMelt web server for nucleic acid melting prediction. *Nucleic Acids Res.* **33**:W577–W581.
73. **Martin, S. L., M. Cruceanu, D. Branciforte, P. W.-L. Li, S. C. Kwok, R. S. Hodges, and M. C. Williams.** 2005. LINE-1 retrotransposition requires the nucleic acid chaperone activity of the ORF1 protein. *J. Mol. Biol.* **348**:549–561.
74. **McCauley, M. J., and M. C. Williams.** 2007. Mechanisms of DNA binding determined in optical tweezers experiments. *Biopolymers* **85**:154–168.
75. **McGhee, J. D.** 1976. Theoretical calculations of the helix-coil transition of DNA in the presence of large, cooperatively binding ligands. *Biopolymers* **15**:1345–1375.
76. **Mirambeau, G., S. Lyonais, D. Coulaud, L. Hameau, S. Lafosse, J. Jeuset, I. Borde, M. Reboud-Ravaux, T. Restle, R. J. Gorelick, and E. Le Cam.** 2007. HIV-1 protease and reverse transcriptase control the architecture of their nucleocapsid partner. *PLoS ONE* **2**:e669.
77. **Mirambeau, G., S. Lyonais, D. Coulaud, L. Hameau, S. Lafosse, J. Jeuset, A. Justome, E. Delain, R. J. Gorelick, and E. Le Cam.** 2006. Transmission electron microscopy reveals an optimal HIV-1 nucleocapsid aggregation with single-stranded nucleic acids and the mature HIV-1 nucleocapsid protein. *J. Mol. Biol.* **364**:496–511.
78. **Morcock, D. R., B. P. Kane, and J. R. Casas-Finet.** 2000. Fluorescence and nucleic acid binding properties of the human T-cell leukemia virus-type 1 nucleocapsid protein. *Biochim. Biophys. Acta* **1481**:381–394.
79. **Narayanan, N., R. J. Gorelick, and J. J. DeStefano.** 2006. Structure/function mapping of amino acids in the N-terminal zinc finger of the human immunodeficiency virus type 1 nucleocapsid protein: residues responsible for nucleic acid helix destabilizing activity. *Biochemistry* **45**:12617–12628.
80. **Nguyen, T. T., A. Y. Grosberg, and B. I. Shklovskii.** 2000. Macroions in salty water with multivalent ions: giant inversion of charge. *Phys. Rev. Lett.* **85**:1568–1571.
81. **Nguyen, T. T., I. Rouzina, and B. I. Shklovskii.** 2000. Reentrant condensation of DNA induced by multivalent counterions. *J. Chem. Phys.* **112**:2562–2568.
82. **Pant, K., R. L. Karpel, I. Rouzina, and M. C. Williams.** 2004. Mechanical measurement of single-molecule binding rates: kinetics of DNA helix-destabilization by T4 gene 32 protein. *J. Mol. Biol.* **336**:851–870.
83. **Pant, K., R. L. Karpel, I. Rouzina, and M. C. Williams.** 2005. Salt dependent binding of T4 gene 32 protein to single and double-stranded DNA: single molecule force spectroscopy measurements. *J. Mol. Biol.* **349**:317–330.
84. **Pant, K., R. L. Karpel, and M. C. Williams.** 2003. Kinetic regulation of single DNA molecule denaturation by T4 gene 32 protein structural domains. *J. Mol. Biol.* **327**:571–578.
85. **Prats, A. C., V. Housset, G. de Billy, F. Cornille, H. Prats, B. Roques, and J. L. Darlix.** 1991. Viral RNA annealing activities of the nucleocapsid protein of Moloney murine leukemia virus are zinc independent. *Nucleic Acids Res.* **19**:3533–3541.
86. **Prats, A. C., L. Sarih, C. Gabus, S. Litvak, G. Keith, and J. L. Darlix.** 1988. Small finger protein of avian and murine retroviruses has nucleic acid annealing activity and positions the replication primer tRNA onto genomic RNA. *EMBO J.* **7**:1777–1783.
87. **Raspaud, E., I. Chaperon, A. Leforestier, and F. Livolant.** 1999. Spermine-induced aggregation of DNA, nucleosome, and chromatin. *Biophys. J.* **77**:1547–1555.
88. **Record, M. T. J., T. M. Lohman, and P. L. de Haseth.** 1976. Ion effects on ligand-nucleic acid interactions. *J. Mol. Biol.* **107**:145–158.
89. **Rein, A., L. E. Henderson, and J. G. Levin.** 1998. Nucleic-acid-chaperone activity of retroviral nucleocapsid proteins: significance for viral replication. *Trends Biochem. Sci.* **23**:297–301.
90. **Rouzina, I., and V. A. Bloomfield.** 1997. Competitive electrostatic binding of charged ligands to polyelectrolytes—practical approach using the non-linear Poisson-Boltzmann equation. *Biophys. Chem.* **64**:139–155.
91. **Rouzina, I., and V. A. Bloomfield.** 1996. Competitive electrostatic binding to DNA. *J. Phys. Chem.* **100**:1977.
92. **Rouzina, I., and V. A. Bloomfield.** 1996. Macroion attraction due to electrostatic correlation between screening counterions. 1. Mobile surface-adsorbed ions and diffuse ion cloud. *J. Phys. Chem.* **100**:9977–9989.
93. **Rouzina, I., K. Pant, R. L. Karpel, and M. C. Williams.** 2005. Theory of electrostatically regulated binding of T4 gene 32 protein to single- and double-stranded DNA. *Biophys. J.* **89**:1941–1956.
94. **Saminathan, M., T. Antony, A. Shirahata, L. H. Sigal, T. Thomas, and T. J. Thomas.** 1999. Ionic and structural specificity effects of natural and synthetic polyamines on the aggregation and resolubilization of single-, double-, and triple-stranded DNA. *Biochemistry* **38**:3821–3830.
95. **Santa Lucia, J., Jr., and D. Hicks.** 2004. The thermodynamics of DNA structural motifs. *Annu. Rev. Biophys. Biomol. Struct.* **33**:415–440.
96. **Shokri, L., B. Marintcheva, C. C. Richardson, I. Rouzina, and M. C. Williams.** 2006. Single molecule force spectroscopy of salt-dependent bacteriophage T7 gene 2.5 protein binding to single-stranded DNA. *J. Biol. Chem.* **281**:38689–38696.
97. **South, T. L., and M. F. Summers.** 1993. Zinc- and sequence-dependent binding to nucleic acids by the N-terminal zinc finger of the HIV-1 nucleocapsid protein: NMR structure of the complex with the Psi-site analog, dACGCC. *Protein Sci.* **2**:3–19.
98. **Stoylov, S. P., C. Vuilleumier, E. Stoylova, H. De Rocquigny, B. P. Roques, D. Gerard, and Y. Mély.** 1997. Ordered aggregation of ribonucleic acids by the human immunodeficiency virus type 1 nucleocapsid protein. *Biopolymers* **41**:301–312.
99. **Tsuchihashi, Z., and P. O. Brown.** 1994. DNA strand exchange and selective DNA annealing promoted by the human immunodeficiency virus type 1 nucleocapsid protein. *J. Virol.* **68**:5863–5870.
100. **Urbaneja, M. A., B. P. Kane, D. G. Johnson, R. J. Gorelick, L. E. Henderson, and J. R. Casas-Finet.** 1999. Binding properties of the human immunodeficiency virus type 1 nucleocapsid protein p7 to a model RNA: elucidation of the structural determinants for function. *J. Mol. Biol.* **287**:59–75.
101. **Urbaneja, M. A., M. Wu, J. R. Casas-Finet, and R. L. Karpel.** 2002. HIV-1 nucleocapsid protein as a nucleic acid chaperone: spectroscopic study of its helix-destabilizing properties, structural binding specificity, and annealing activity. *J. Mol. Biol.* **318**:749–764.
102. **Vijayanathan, V., T. Thomas, A. Shirahata, and T. J. Thomas.** 2001. DNA condensation by polyamines: a laser light scattering study of structural effects. *Biochemistry* **40**:13644–13651.
103. **Vladescu, I. D., M. J. McCauley, I. Rouzina, and M. C. Williams.** 2005. Mapping the phase diagram of single DNA molecule force-induced melting in the presence of ethidium. *Phys. Rev. Lett.* **95**:158102.
104. **Vo, M. N., G. Barany, I. Rouzina, and K. Musier-Forsyth.** 2006. Mechanistic studies of mini-TAR RNA/DNA annealing in the absence and presence of HIV-1 nucleocapsid protein. *J. Mol. Biol.* **363**:244–261.
105. **Vuilleumier, C., E. Bombarda, N. Morellet, D. Gerard, B. P. Roques, and Y. Mély.** 1999. Nucleic acid sequence discrimination by the HIV-1 nucleocapsid protein NCp7: a fluorescence study. *Biochemistry* **38**:16816–16825.
106. **Wetmur, J. G., and N. Davidson.** 1968. Kinetics of renaturation of DNA. *J. Mol. Biol.* **31**:349–370.
107. **Williams, M. C., R. J. Gorelick, and K. Musier-Forsyth.** 2002. Specific zinc-finger architecture required for HIV-1 nucleocapsid protein's nucleic acid chaperone function. *Proc. Natl. Acad. Sci. USA* **99**:8614–8619.

108. **Williams, M. C., and I. Rouzina.** 2002. Force spectroscopy of single DNA and RNA molecules. *Curr. Opin. Struct. Biol.* **12**:330–336.
109. **Williams, M. C., I. Rouzina, and V. A. Bloomfield.** 2002. Thermodynamics of DNA interactions from single molecule stretching experiments. *Acc. Chem. Res.* **35**:159–166.
110. **Williams, M. C., I. Rouzina, J. R. Wenner, R. J. Gorelick, K. Musier-Forsyth, and V. A. Bloomfield.** 2001. Mechanism for nucleic acid chaperone activity of HIV-1 nucleocapsid protein revealed by single molecule stretching. *Proc. Natl. Acad. Sci. USA* **98**:6121–6126.
111. **You, J. C., and C. S. McHenry.** 1993. HIV nucleocapsid protein. Expression in *Escherichia coli*, purification, and characterization. *J. Biol. Chem.* **268**:16519–16527.
112. **Zhou, J., R. L. Bean, V. M. Vogt, and M. Summers.** 2007. Solution structure of the Rous sarcoma virus nucleocapsid protein: muPsi RNA packaging signal complex. *J. Mol. Biol.* **365**:453–467.
113. **Zhou, J., J. K. McAllen, Y. Taylor, and M. F. Summers.** 2005. High affinity nucleocapsid protein binding to the muPsi RNA packaging signal of Rous sarcoma virus. *J. Mol. Biol.* **349**:976–988.
114. **Zuker, M.** 2003. Mfold web server for nucleic acid folding and hybridization prediction. *Nucleic Acids Res.* **31**:3406–3415.